Distinct TDP-43 aggregate features and toxicity stratify FTD patients

Laferrière Florent[1*], Maniecka Zuzanna[1*], Pérez-Berlanga Manuela[1], Hruska-Plochan Marian[1], Gilhespy Larissa[1], Hock Eva-Maria[1], Wagner Ulrich[2], Afroz Tariq[1], Boersema Paul J.[3], Gery Barmettler[4], Foti Sandrine C.[5,6], Asi Yasmine T.[5,6], Isaacs Adrian M.[6,7], Al-Amoudi Ashraf[8], Lewis Amanda[8], Stahlberg Henning[8], Ravits John[9], De Giorgi Francesca[10,11,12], Ichas François[10,11,12], Bezard Erwan[11,12], Picotti Paola[4], Lashley Tammaryn[5,6], Polymenidou Magdalini[1]

[1]Institute of Molecular Life Sciences, University of Zurich, Winterthurerstrasse 190, CH-8057 Zurich, Switzerland

[2]Department of Pathology and Molecular Pathology, University Hospital Zurich, CH-8091 Zurich, Switzerland

[3]Institute of Biochemistry, Department of Biology, ETH Zurich (ETHZ), CH-8093 Zurich, Switzerland

[4]Center for Microscopy and Image Analysis, University of Zurich, CH-8057 Zurich, Switzerland

[5]Queen Square Brain Bank for Neurological diseases, Department of Movement Disorders, UCL Institute of Neurology, London, WC1N 1PJ, UK

[6]Department of Neurodegenerative Disease, UCL Institute of Neurology, Queen Square, London, WC1N 3BG, UK

[7]UK Dementia Research Institute at UCL, UCL Institute of Neurology, Queen Square, London, WC1N 3BG, UK

[8]Center for Cellular Imaging and NanoAnalytics (C-CINA), Biozentrum, University of Basel, CH-4058 Basel, Switzerland

[9]Department of Neuroscience, University of California, San Diego, 9500 Gilman Drive, La Jolla, CA, 92093-0624, USA

[10]INSERM U1084, Laboratoire des Neurosciences Expérimentales et Cliniques, Université de Poitiers, 86073 Poitiers, France

[11]Université de Bordeaux, Institut des Maladies Neurodégénératives, UMR 5293, 33076 Bordeaux, France

[12]CNRS, Institut des Maladies Neurodégénératives, UMR 5293, F-33076, Bordeaux, France

*These authors contributed equally to this work

Author for correspondence:

Magdalini Polymenidou, PhD
Institute of Molecular Life Sciences, Y32-J06
University of Zurich
Winterthurerstrasse 190,
CH-8057 Zurich
Office: +41-44-635-3106
Cell: +41-79-137-6856
email: magdalini.polymenidou@imls.uzh.ch

Keywords – ALS, FTD, FTLD, TDP-43, protein aggregation, neurotoxicity, prion-like seeding

Abstract

Accumulation of abnormally phosphorylated TDP-43 (pTDP-43) is the main pathology in affected neurons of patients with amyotrophic lateral sclerosis (ALS) and frontotemporal dementia (FTD). Morphological diversity and neuroanatomical distribution of pTDP-43 accumulations allowed classification of FTD cases into at least four different subtypes, which correlate with clinical presentations and genetic causes. To understand the molecular basis of this heterogeneity, we developed SarkoSpin, a new method for extremely pure biochemical isolation of pathological TDP-43. Combining SarkoSpin with mass spectrometry, we revealed proteins beyond TDP-43, which become abnormally insoluble in a disease subtype-specific manner. We show that pTDP-43 extracted from disease brain forms large and stable assemblies of distinct densities and morphologies that correlate with disease subtypes. Importantly, biochemically extracted pTDP-43 assemblies displayed differential neurotoxicity and seeding that correlated with disease duration of FTLD patients. Our data indicate that disease heterogeneity may originate from alternate pathological TDP-43 conformations, reminiscent of prion strains.

Introduction

Amyotrophic lateral sclerosis (ALS) and frontotemporal dementia (FTD) are neurodegenerative disorders thought to represent the two ends of a disease spectrum, due to their genetic, pathological and clinical overlap[1]. ALS is the most common form of motor neuron disease (MND), affecting upper and lower motor neurons and ultimately leading to progressive paralysis. FTD is the second most common form of dementia after Alzheimer's disease[2] and is characterized by severe atrophy of frontal and temporal lobes and is, therefore, also referred to as frontotemporal lobar degeneration (FTLD). Approximately 10% of ALS and 40% of FTD cases are familial and are associated with mutations in a large number of genes[1,3], the most common of which are hexanucleotide repeat expansions on chromosome 9 open reading frame 72 gene (*C9ORF72*)[4,5]. The remaining cases are sporadic with apparent lack of family history.

The major common hallmark of these two diseases is the presence of pathological, ubiquitinated protein inclusions in affected neurons, which in almost all ALS and about 45% of FTD patients primarily contain the RNA/DNA-binding protein TDP-43 (Transactivation Response DNA Binding Protein of 43 kDa)[6,7]. TDP-43 is a member of the heterogeneous nuclear ribonucleoprotein (hnRNP) family[8] and it plays essential roles in splicing regulation[9,10] which are dependent on the formation of physiological TDP-43 oligomers[11,12,13]. TDP-43 is predominantly nuclear, but it can shuttle to the cytoplasm[14], where it incorporates into stress[15] and transporting RNA[16,17] granules via its low complexity domain (LCD), which mediates phase separation[18,19].

FTLD- and ALS-associated pathological TDP-43 was shown to undergo several abnormal post-translational modifications including poly-ubiquitination, hyper-phosphorylation and proteolytic cleavage[6,7]. The latter leads to the formation of a highly aggregation-prone C-terminal fragment of 25 kDa that is deposited in the inclusions along with the full-length TDP-43[20,21]. Notably, the majority of ALS-linked mutations are localized within this C-terminal LCD[22,1] and were shown to increase TDP-43 aggregation propensity[23,24] without directly affecting its function in RNA splicing[25]. Rather, aggregate

formation and mislocalization of mutant or, most frequently, the wild type protein are thought to trigger two non-exclusive toxic mechanisms: loss of its normal function and gain of aggregate toxicity[26].

While ALS presents with rather unified TDP-43 neuropathology, FTLD is more heterogeneous and manifests with diverse histological patterns. The latter correlate with various clinical presentations, including behavioral variant FTD (bvFTD), semantic dementia (SD) and primary non-fluent aphasia (PNFA), as well as genetic mutations[27]. Based on the morphology and neuroanatomical distribution of pathological TDP-43 accumulations, FTLD-TDP can be classified into the following distinct subtypes[28,29]. FTLD-TDP type A (FTLD-TDP-A) is characterized by neuronal cytoplasmic inclusions (NCI), dystrophic neurites (DN) and neuronal intranuclear inclusions (NII) in upper cortical layers and typically manifests with bvFTD but no MND. Some FTLD-TDP-A patients carry *GRN* or *C9ORF72* mutations, which are non-distinguishable from sporadic cases based on TDP-43 pathology. FTLD-TDP type B cases (FTLD-TDP-B), which can also be linked to *C9ORF72* mutations, show primarily granular NCI expanding across all cortical layers, and present with a combination of FTD and MND. Finally, FTLD-TDP type C (FTLD-TDP-C) comprises long and thick DN and few NCI primarily in the superficial cortical layers. These cases are sporadic and present with SD without MND. Recently, other subtypes, which do not fully adhere to these pathological classification criteria were described[28,29], suggesting that we are only beginning to identify the full spectrum of disease heterogeneity. The origin of this pathological diversity, which is associated with specific clinical presentations[30] remains unknown, but was proposed to correlate with specific molecular signatures[31,32].

In order to address the molecular underpinnings of disease heterogeneity, we sought to analyze the biochemical and physical characteristics of TDP-43 aggregates such as size, shape, density and composition. The first and mandatory step in this characterization is the isolation of pathological assemblies and their physical separation from physiological TDP-43 and similar proteins. Currently, there is no reliable method for native extraction of TDP-43 aggregates for the analysis of pathological TDP-43 conformation, aggregation status, neurotoxicity and seeding potential. To achieve this, we

developed SarkoSpin, a novel and simple extraction method for physical separation of pathological TDP-43 from more than 99% of total protein mass including the extreme bulk of physiological, monomeric and oligomeric[11] TDP-43. Using SarkoSpin on brain cortical samples from over 80 patients, we found that TDP-43 forms large and buoyant assemblies of distinct densities, polyubiquitination levels and morphologies that correlate with specific neuropathological classifications. Importantly, coupling SarkoSpin with mass spectrometry, we illustrate that a specific subset of proteins, beyond TDP-43, become insoluble in each disease subtype. These proteins are rarely co-aggregated with pTDP-43 and most likely represent a downstream effect of TDP-43 pathology. One of these proteins depicts a distinct astrocytic reaction discriminating FTLD-TDP-A from FTLD-TDP-C patients, illustrating divergent pathogenic mechanisms within these two disease subtypes. Most importantly, we show evidence that SarkoSpin extracted pTDP-43 assemblies exhibit cytotoxicity and protein seeding ability. Remarkably, pathological aggregates extracted from FTLD-TDP-A were significantly more cyto- and neurotoxic than those extracted from FTLD-TDP-C, thereby correlating with the significant difference in disease duration between these two subtypes. Collectively, our data demonstrate that ALS and FTLD heterogeneity is consistently reflected in the biochemical, neurotoxic and seeding properties of TDP-43 and the associated insoluble proteome. We propose that alternative TDP-43 pathological conformations may underlie the diversity of TDP-43 proteinopathies, reminiscent of prion strains[33,34].

Results

Summary of patient cohort and characterization of FTLD-TDP-A and FTLD-TDP-C cases

Brain cortical samples from over 80 patients, including control patients with no apparent CNS pathology or with non-TDP-43-linked neurodegeneration, as well as ALS and FTLD patients of different subtypes (from both sporadic and genetic origins) were obtained from the University of California in San Diego (USA), the Queen Square Brain Bank for Neurological Disorders, University College London (UK), and the Netherlands Brain Bank (**Supplementary Table 1**). The morphology

and neuroanatomical distribution of pathological TDP-43 accumulations of cases used in this study adhered to the current classifications[28,29]. FTLD-TDP-A cases were primarily characterized by NCI with few, short DN and NCI in upper cortical layers, a pattern that was indistinguishable in sporadic or patients with *C9ORF72* mutations (**Supplementary Fig. 1a**). In contrast, FTLD-TDP-C cases, which were exclusively sporadic and did not develop MND, harbored long DN and few NCI, primarily in the superficial cortical layers (**Supplementary Fig. 1a**). Furthermore, it was recently reported that FTLD-TDP-C patients show significantly longer disease duration compared to all other subtypes[29], which we could also confirm in our cohort (**Supplementary Fig. 1b-c**).

SarkoSpin: a new method for the isolation of pathological TDP-43 from human brain

Although pathological TDP-43 is resistant to detergents, such as sarkosyl[35,36,31,37], there is currently no method that allows the physical separation of pathological TDP-43 from the pool of other proteins in complex tissues. In fact, physiological TDP-43, as well as other proteins containing low complexity domains, typically co-purify with pathological TDP-43 in the sarkosyl-insoluble fractions from patient brain tissue[36,37] (**Supplementary Fig. 2a-b**). This contamination is likely due to the formation of large complexes with nucleic acids, including physiological nuclear TDP-43 oligomers[11], which become partially resistant to detergent solubilization (**Supplementary Fig. 2b**).

To overcome this limitation and to purify pathological TDP-43 from its normal counterpart bound to nucleic acids, we combined harsh solubilization with nuclease treatment and a single centrifugation step, in a new method we termed SarkoSpin (**Fig. 1a-b**). In order to assess the efficiency of our technique, we analyzed motor and frontal cortex homogenates from six controls, six ALS, six FTLD-TDP-A, three FTLD-TDP-B and six FTLD-TDP-C (**Supplementary Table 1**). Total protein amounts partitioning in the SarkoSpin supernatant and pellet fractions were estimated by silver staining of SDS-PAGE analyzed samples (**Fig. 1c** and **Supplementary Fig. 2c**) and by measuring protein concentrations. On average, 99.8% of the total protein mass resided in the supernatant with no significant difference between disease and control, or between disease types (**Fig. 1d**). 99.9% of total

TDP-43 was found in the supernatants of control samples (**Fig. 1e-f** and **Supplementary Fig. 3**). The monoclonal anti-TDP-43 antibody used (#60019-2-Ig), also non-specifically binds to a faster migrating band (<40 kDa), which was not detected by a panel of anti-TDP-43-specific antibodies (**Supplementary Fig. 4**). Interestingly, in disease cases, only 88% of total TDP-43 was found in supernatants, indicating that the rest of TDP-43 was present in the sarkosyl-insoluble pellet and corresponds to the pathological species. Indeed, the pellet fraction in these cases presented a clear signature characteristic for pathological TDP-43, namely poly-ubiquitination, C-terminal cleavage and hyperphosphorylation, detected as a higher molecular weight band (~50 kDa) seen by a total TDP-43 antibody (**Fig. 1b, e, f** and **Supplementary Fig. 3**). The latter, detected strongly by a specific antibody against phosphorylated TDP-43 (pS409/410), shows great enrichment of pathological TDP-43 exclusively in disease pellets (**Fig. 1g**) at an average of 64% with no significant difference between disease types (**Fig. 1h**). Based on this analysis, we estimate that the average percentage of total TDP-43 that is phosphorylated on serine residues 409/410 in patient samples is 12% with wide inter-individual variation and no significant difference between disease types (**Supplementary Fig. 5a**).

Proteins with low-complexity domains or RNA/DNA binding ability, such as other members of the hnRNP family, as well as other ALS/FTD-associated proteins (FUS, hnRNPA1, hnRNPH, SOD1) and normal proteins partitioning in complex macromolecular assemblies (actin, histones), were virtually absent in SarkoSpin pellets (**Fig. 1i** and **Supplementary Fig. 3**). More than 99.8% of each of these proteins was found in SarkoSpin supernatants of all samples tested (**Fig. 1j**). Taken together, these data demonstrate that SarkoSpin allows the strict isolation of pathological TDP-43 and its physical separation from the vast majority of physiological TDP-43 and other proteins, including those with nucleic acid binding ability, low complexity domains and/or high aggregation propensity.

SarkoSpin captures native pathological TDP-43 assemblies

To further characterize the properties of these assemblies, we next performed native PAGE electrophoresis of SarkoSpin supernatants and pellets from control and disease cases. Total TDP-43

native blots on SarkoSpin supernatants of all cases including controls showed a wide smear, ranging from the stacking gel (>10 MDa) to the size of monomeric TDP-43, where a strong band was observed (**Supplementary Fig. 6**, top left panel). TDP-43 is therefore present in different oligomeric states in all samples, in agreement with our recent report[11]. Notably, total protein concentrations were equalized before SarkoSpin, explaining the overall lower signal observed in the control lane, which lack accumulated TDP-43 aggregates.

Strikingly, a strong TDP-43 signal was detected in the stacking gel in the patient but not in the control samples. When immunoblotted with pTDP-43-specific antibody, only this particular high molecular weight signal was detected (**Supplementary Fig. 6** top right panel), indicating that it corresponds to the pathological species. Importantly, in contrast to control samples, SarkoSpin-pelleted patient samples immunoblotted with total TDP-43- or pTDP-43-specific antibodies revealed solely the presence of high molecular weight assemblies retained in the stacking gels and complete absence of monomeric or oligomeric TDP-43 (**Supplementary Fig. 6**, lower panels), further confirming the efficient separation of pathological from physiological assemblies. If exclusively composed of TDP-43, such high ordered aggregates would consist of at least 200 monomers, which may represent the minimal unit comprising the large inclusions found in patient-affected neurons. No differences were observed among the various disease types. However, it cannot be excluded that subtype-specific differences occur above the resolved sizes, undetectable by the resolution of this assay.

Insoluble proteome and levels of pathological TDP-43 ubiquitination distinguishes disease subtypes

To explore which other proteins, beyond TDP-43, become insoluble in patient samples, we analyzed SarkoSpin preparations from brain homogenates of eleven controls, three FTLD-Tau, six ALS or FTD-ALS, nine FTLD-TDP-A, three FTLD-TDP-B and six FTLD-TDP-C by liquid chromatography-mass spectrometry (LC-MS). SarkoSpin pellets were denatured with 8 M Urea and protein concentration was equalized across the samples prior to enzymatic digestion and LC-MS analysis. Samples were

measured on a high-resolution mass spectrometer and the acquired tandem mass spectra were searched against human protein database. Spectral counting was used for quantifying differences in protein abundance between the different samples. The most significantly enriched protein ($p = 10^{-3}$) and most consistently correlating ($r = 0.65$) with patient, but not control or FTLD-Tau, SarkoSpin pellets was TDP-43 (**Supplementary Fig. 7**), in accordance with previous studies[7,6]. All remaining proteins had weaker correlation values ($r < 0.5$) and were less consistently enriched in the patient group, illustrating that indeed TDP-43 is the main component of insoluble protein aggregates and further validating SarkoSpin as a reliable method for their isolation.

Importantly, when we compared the insoluble proteins enriched in each disease group separately (**Supplementary Fig. 8-11**), we found that a distinct set of proteins characterized each subtype (**Fig. 2a**). This suggests that while TDP-43 is the only protein consistently converting into an aggregated form in all disease cases tested, a specific subclass of proteins accompany TDP-43 within the insoluble fraction of each individual disease group. A few of these proteins such as LAMA1 and HepaCAM belong to the extracellular matrix and most probably associate with TDP-43 after tissue lysis due to their high abundance and adhesive nature. Conversely, all other proteins found in patient SarkoSpin pellets are localized intracellularly and might be interacting with aggregating TDP-43 within affected neurons.

To confirm these findings, we first tested a number of commercially available antibodies for sensitivity and specificity to several of the protein targets, predicted to correlate with pTDP-43 levels in specific disease subtypes by our analysis (**Fig. 2a**). Based on their performance, we selected one protein per disease group, namely: profilin 1 (PFN1), which we found enriched in ALS cases and was previously reported to be mutated in rare familial ALS cases[38,39], N-acylsphingosine amidohydrolase (ASAH1), enriched in FTLD-TDP-A cases and reported to be mutated in some cases of spinal muscular atrophy[40] and Thioredoxin-like protein 1 (TXNL1), enriched in FTLD-TDP-C in our dataset. We then tested their presence in SarkoSpin fractions of individual patients by immunoblot and found that, while their levels were comparable on SarkoSpin supernatants (**Supplementary Fig. 12a-b**), they were

enriched in the pellets of samples from TDP-43 proteinopathies (**Fig. 2b**). Notably, this enrichment best correlated with pTDP-43 levels in the respective disease subtype (**Fig. 2c**), in agreement with our mass spectrometry results. Despite the large variability in pTDP-43 levels of individual patient samples, we confirmed the validity of these correlations, by the almost perfect correlation for all groups with total TDP-43 in these pellets (**Supplementary Fig. 12c-d**), as expected.

A similar approach was used to correlate ubiquitin and pTDP-43 levels in SarkoSpin pellets, which revealed an interesting and unexpected observation. Ubiquitin blots of SarkoSpin pellets and supernatants showed a completely different pattern, with ubiquitin-positive smears characteristic for pathological polyubiquitination present only in the pellets (**Fig. 2d**). This confirmed that SarkoSpin specifically concentrated aggregated and misfolded proteins that escape the proteasome degradation pathway in neurodegeneration. Surprisingly, however, the ubiquitin levels of pTDP-43 extracted from FTLD-TDP-C patients were consistently lower than those derived from FTLD-TDP-A and ALS patients (**Fig. 2d-e**). Comparison of co-immunofluorescence analysis of pTDP-43 and ubiquitin on postmortem brain sections of FTLD-TDP-A and FTLD-TDP-C patients confirmed the differential levels of pTDP-43 polyubiquitination (**Fig. 2f-g** and **Supplementary Fig. 12e**), consistent with distinct molecular mechanisms generating pathology in these two disease subtypes.

To investigate if the increased insolubility of ASAH1 and TXNL1 resulted from direct co-aggregation with pTDP-43, or if these proteins become insoluble as a downstream event of TDP-43 aggregation, similar to what has been shown in other protein aggregation diseases[41], we performed co-immunofluorescence analysis with pTDP-43 on control, FTLD-TDP-A and FTLD-TDP-C brain sections. ASAH1 and TXNL1 both demonstrated cytoplasmic staining, which was increased in levels and displayed a punctate pattern in both patient subtypes (**Supplementary Fig. 13**). This pattern appeared largely independent of pTDP-43 inclusions, with rare co-localization observable in both disease subtypes. This suggested that increased insolubility of these proteins in disease does not result from direct interaction and co-aggregation with pTDP-43 and that SarkoSpin likely dissociated

other proteins previously shown to co-aggregate with pTDP-43 on patient tissues[42], thereby releasing the pTDP-43 "core" of these pathological assemblies**.**

Importantly, one of the proteins enriched in the FTLD-TDP-A group in our mass spectroscopy analysis was the F-Box Protein 2 (FBXO2), which during our initial screen by conventional immunohistochemistry stained neuronal cytoplasm in control and FTLD-TDP-C brain sections, while in the FTLD-TDP-A subtype a characteristic astrocytic-like pattern was observed (**Supplementary Fig. 14a**). To further explore this finding, we performed co-immunofluorescence analysis of FBXO2 and the astrocytic marker glial fibrillary acidic protein (GFAP). Excitingly, while in both disease subtypes astrogliosis was evident by the increased GFAP staining, FBXO2 marked FTLD-TDP type A, but not type C astrocytes (**Fig. 2h** and **Supplementary Fig. 14b**). These data indicate a previously unrecognized distinct astrocytic reaction characterizing FTLD-TDP-A patients, once again illustrating divergent pathogenic mechanisms within these two disease subtypes. In conclusion, the individual signatures of insoluble protein ensembles within each disease subtype, as well as the differential level of pTDP-43 polyubiquitination likely reflect distinct pathological processes, despite the coinciding TDP-43 aggregation.

Diverse size distributions of TDP-43 aggregates isolated from different types of TDP-43 proteinopathies

In order to further understand the differences in protein composition of TDP-43 aggregates and to explore the molecular basis underlying disease subtypes, we assessed the sedimentation profiles of TDP-43 aggregates to uncover specific size or shape differences. Brain cortex homogenates of eight controls, two ALS and two FTD-ALS (pooled in a single ALS group), eleven FTLD-TDP-A, three FTLD-TDP-B and nine FTLD-TDP-C were SarkoSpin-solubilized and layered on top of a linearized 10-25% iodixanol continuous gradient before ultracentrifugation (310,000 g) for 45 minutes at 4°C (**Fig. 3a**). The gradients were then fractionated in 16 fractions of equal volume and TDP-43 or pTDP-43 distribution was assessed by immunoblot or dot blot using the respective antibodies. In both

control and disease samples monomeric, as well as oligomeric TDP-43, were retained in the top five fractions, peaking in the first three (**Fig. 3b-d** and **Supplementary Fig. 15-16**). In addition, in disease, but not in control samples, populations of larger sizes were identified, carrying the specific post-translational modifications of pathological TDP-43. In ALS samples, sedimentation profiles revealed one population of aggregated and phosphorylated TDP-43 in fractions 8 to 13 and peaking between 10-11. FTLD-TDP-A sedimentations revealed a wide diversity of profiles, with TDP-43 aggregates sedimenting in fractions 5 to 14, and two apparent populations peaking in fractions 6-7 and in fraction 11. The presence of a second subpopulation could indicate a difference in size or shape of the aggregates. Type A cases used in this study were separated in three different subgroups according to their genetic background: sporadic (with no familial history and no known mutations identified), *GRN* and *C9ORF72*, while all FTLD-TDP-B cases carried *C9ORF72* mutations. Despite slight differences in the relative distribution of aggregates, with the *GRN* patients favoring the larger TDP-43 populations, no striking patterns separating the three groups of patients classified as type A (**Supplementary Fig. 17**), Importantly, neuropathological type rather than *C9ORF72* mutation better correlated with the size distribution of TDP-43 aggregates, as they followed the pattern observed for the respective disease type (peaks in fractions 6-7 and 11 for type A and fractions 10-12 for type B) and clearly separated in different groups.

Moreover, FTLD-TDP-C sedimentation profiles also revealed one broad population of TDP-43 aggregates (**Fig. 3b-c** and **Supplementary Fig. 15-16**). However, in contrast to the other types, these assemblies were sedimenting further, in fractions 10-16, which may indicate that they were of bigger size and/or that their intrinsic density is higher. Purified recombinant human TDP-43 protein expressed in *E. coli* and aggregated *in vitro* concentrated in fractions 11-13, showing distinct properties from all patient-derived aggregates (**Supplementary Fig. 18a-b**). Importantly, hnRNPA1, FUS and SOD1 remained in the first three fractions in all disease types, indistinguishable from controls (**Supplementary Fig. 19**), indicating that the solubility of these proteins is not significantly altered in TDP-43 proteinopathies.

315 Furthermore, taking into account that the top five fractions correspond to the physiological TDP-43,
316 while fractions 6 to 16 contain only the pathological assemblies, the percentage of aggregated TDP-
317 43 could be calculated for each individual patient (**Supplementary Fig. 5b**) and was found between
318 20-30% depending on the disease group. Levels of aggregated TDP-43 followed a similar trend as
319 phosphorylated TDP-43 (**Supplementary Fig. 5a**), with FTLD-TDP-C being the highest, followed by
320 FTLD-TDP-A and then ALS, albeit these differences did not reach statistical significance. The
321 observation that there is more aggregated than phosphorylated TDP-43 (**Supplementary Fig. 5a-b**)
322 indicates that not all aggregated TDP-43 was phosphorylated, and potentially also that not all
323 pathological phosphorylation occurred at amino acids S409/410.
324
325 **Distinct density profiles of TDP-43 aggregates isolated from different types of TDP-43**
326 **proteinopathies**
327 To determine whether the observed differences in velocity sedimentation are due to distinct aggregate
328 size, shape or density, we sought out to measure the intrinsic density of TDP-43 aggregates by
329 combining our SarkoSpin solubilization conditions with density floatation gradients[33]. To this end, we
330 submitted the same patient samples to SarkoSpin solubilization, followed by ultracentrifugation
331 (125,000 g) in a 10-60% iodixanol discontinuous gradient for 17 hours at 4°C to reach the isopycnic
332 equilibrium (**Fig. 4a**). The gradients were then fractionated and TDP-43 and pTDP-43 density profiles
333 were determined as described above (**Fig. 4b-d** and **Supplementary Fig. 20-21**).
334 In all samples, the majority of normal TDP-43 was present in one peak spanning fractions 8 to 12, i.e.
335 at an average density of 1.22 g/mL, as calculated by refractometry and iodixanol concentration
336 (**Supplementary Fig. 22**). Remarkably, all density gradients from ALS, FTLD-TDP-A (**Fig. 4b-c**) as
337 well as FTLD-TDP-B cases (**Supplementary Fig. 20a**) showed an additional population of TDP-43,
338 present in one sharp peak in fraction 7, corresponding to density of 1.16 g/mL. This consistent
339 population demonstrates all known TDP-43 pathological features such as ubiquitination, C-terminal
340 cleavage, and phosphorylation (**Supplementary Fig. 21a-b**). Notably, pTDP-43 was not detected on

dot blots or immunoblots of all control density gradients, showing the specificity of the S409/410 phosphorylation site as a marker of pathological TDP-43. The lower density of pathological TDP-43 compared to the main population of its physiological counterpart is likely determined by the three-dimensional packing of these aggregates, rather than their direct association with lipids, as the purified human recombinant TDP-43 aggregates reconstituted *in vitro*, showed exactly the same density (**Supplementary Fig. 18c-d**).

Surprisingly, the density profiles of all nine FTLD-TDP-C samples were significantly different from all other types of TDP-43 proteinopathies tested. The FTLD-TDP-C pathological TDP-43 population was intermingled with the normal TDP-43 peak in denser fractions 8 to 10, i.e. 1.20 g/mL (**Fig. 4b-c**, **Supplementary Fig. 20b, Supplementary Fig. 21b**). These results strikingly show that pathological TDP-43 aggregates extracted from FTLD-TDP-C were ordered in a different fashion than those found in other FTLD-TDP subtypes or ALS. Therefore, the distinct histopathological profiles and clinical symptoms described for this subtype were directly correlated with this specific molecular signature.

Alternate morphologies of TDP-43 aggregates isolated from different disease subtypes

To further characterize the properties and structural differences of these assemblies, we performed native PAGE immunoblots on density floatation gradient fractions from control and patient samples. Control density gradients were totally devoid of pTDP-43 signal, whereas the high molecular weight pTDP-43 aggregates described previously were present in fraction 7 and 8-10 for FTLD-TDP-A and FTLD-TDP-C, respectively (**Supplementary Fig. 23** green and blue arrows), in accordance with previous findings (**Fig. 4**). In addition to the pathological TDP-43 aggregates, two major populations of assemblies were distinguishable in all cases, including controls: one in fractions 8 to 12 under 66 kDa, and one in fractions 5 to 7 smearing from 66 kDa to 10 MDa. The latter was composed of a wide diversity of TDP-43 oligomers[11], which were more buoyant than monomeric species. We estimated that under these conditions approximately 25-35% of total TDP-43 appears to be oligomeric in controls (**Supplementary Fig. 5c**). This further demonstrated that in diseased brains, TDP-43 is

present in different distinguishable arrangements: monomers, oligomers of different sizes and larger aggregates.

As the resolution of native PAGE electrophoresis did not allow for a precise definition of their sizes, extracted aggregates were subjected to filtration, to define whether these particles were smaller than 220 nm, and if so, to further characterize them using electron microscopy (see below). SarkoSpin supernatants and pellets of all samples were subjected to syringe low-retention 0.22 µm filtration, prior to dot blotting with TDP-43, pTDP-43 and hnRNPA1-specific antibodies (**Supplementary Fig. 24a**), without altering the relative partition of different proteins in supernatant or pellet fractions. Surprisingly, the majority of TDP-43 aggregates were recovered after filtration, as confirmed by positive pTDP-43 signal on dot blots of filtered SarkoSpin pellets. Filtration resulted in an average reduction of pTDP-43 signal of 33% and 36% in FTLD-TDP-A and FTLD-TDP-C SarkoSpin pellets, respectively (**Supplementary Fig. 24b**). The reduction of total TDP-43 due to filtration of pellets was lower, with 20% and 30% respectively. Normal TDP-43 and hnRNPA1 were not retained in the filter as they showed signal reduction of less than 10% for all cases with no significant difference between control and disease samples. These results demonstrate that around 70% of TDP-43 pathological aggregates are smaller than 220 nm for all disease groups. Combined with the velocity sedimentation profiles, in which 70% of sedimenting TDP-43 showed an estimated size of 220 nm, the median size separating the Gaussian-like repartition of aggregated TDP-43 in two equal populations would be on average ~150 nm.

In order to visualize TDP-43 aggregates, anti-TDP-43 immunogold labeling followed by transmission electron microscopy was performed on filtered SarkoSpin pellets of control, FTLD-TDP-A and FTLD-TDP-C cases (**Fig. 5a**). To avoid drying artifacts common in standard negative-stain EM, samples were embedded in methylcellulose. No immunoreactivity or large protein assemblies could be detected in control samples. In contrast, FTLD-TDP-A and FTLD-TDP-C SarkoSpin pellets contained numerous protein structures of various shapes and sizes, ranging from 50 to 150 nm, which were decorated by gold bead-labeled anti-TDP-43 antibody (**Fig. 5a**, red arrows). Interestingly, although the

same monoclonal antibody recognizing a short epitope spanning amino acids 203-209 under denaturing conditions did not show consistent differences between the two disease groups, immunogold-EM revealed differential immunoreactivity between the two disease subtypes. Assemblies isolated from FTLD-TDP-A patients were strongly immuno-positive whereas those extracted from FTLD-TDP-C cases were only sparsely labeled by the same antibody. This lower antibody detection points to distinct epitope accessibility, and thus different packaging of pathological TDP-43 type A versus type C aggregates. It is conceivable that the antibody epitope, which lies within the second RNA recognition motif (RRM2), is buried inside the core of FTLD-TDP-C aggregates. These results corroborate the higher density of type C aggregates and further confirm their discriminating three-dimensional shapes compared to type A.

Notably, we did not detect any long amyloid fibrils in any disease case, in agreement with the apparent lack of amyloidophilic staining in the majority of ALS/FTD patient brains[43,44]. Nevertheless, careful observation of the immunogold-EM images suggested the presence of short proteinaceous filaments of a thickness of 5 to 8 nm, and a length of 30 to 50 nm, which were frequently decorated by the anti-TDP-43 antibody in FTLD-TDP-A cases (**Fig. 5a**, orange arrows). Similar structures were detected in FTLD-TDP-C samples, albeit mostly independent from antibody labeling (**Fig. 5b**, orange arrows). These structures potentially originated from filamentous material in FTLD brains as previously reported[45], which would be in agreement with a recent study showing high-resolution structure of a short TDP-43 fragment residing in its LCD[46].

As the use of methylcellulose lowers the image resolution, immunolabelled SarkoSpin pellets prepared without this preservation step were also analyzed by transmission electron microscopy. This allowed us to obtain higher resolution images of type A TDP-43 aggregates. These showed heterogenous spheroid or elongated and coiled protein assemblies (**Fig. 5c**). Due to lower immunoreactivity, such structures could not be identified in type C samples. Importantly, both methods for immunogold-labeled sample preparation, with or without methylcellulose, showed no unspecific binding of the gold-conjugated secondary antibody in the absence of TDP-43 primary

antibody (**Supplementary Fig. 25a**). The presence of lipids that sometimes appeared adjacent to the TDP-43 aggregate structures (**Fig. 5a**, yellow arrows) could be efficiently removed by a slight adaptation of our SarkoSpin method with centrifugation over a sucrose cushion (**Supplementary Fig. 25b**).

To obtain an independent, albeit indirect, measure of the different conformational features of TDP-43 aggregates we used partial proteolysis. The latter has extensively been used as a surrogate for probing different pathological conformations of the prion protein, since the size of the proteolytic fragments is directly related to the specific site that is accessible to the chosen protease[34,47]. In contrast to the prion protein, TDP-43 is largely proteinase K-sensitive (**Supplementary Fig. 25c**), but has previously been reported to be partially resistant to chymotrypsin and trypsin[31,32]. Here, we systematically analyzed the proteolytic profile of TDP-43 species extracted from different disease subtypes (**Fig. 5d**). Indeed, chymotrypsin and trypsin-treated SarkoSpin pellets showed specific and consistent proteolytic profiles in each disease subtype, suggesting that the arrangement of these aggregates and, by extension, the borders of the protease-resistant cores are distinctive. Additionally, probing with antibodies raised against defined TDP-43 domains revealed resistance of the most C-terminal fragment within the low-complexity domain, suggesting that the cleavage site is hidden within the core of the aggregates. Interestingly, these were found to be significantly more resistant to proteolysis by trypsin in FTLD-TDP-C compared to type A (**Fig. 5e**). Lastly, we explored this proteolytic resistance of TDP-43 species to visualize the resistant cores of the aggregates, which we identified using immunogold labeling with an antibody against the TDP-43 phosphorylation sites at amino acids 409/410 (**Fig. 5f**). This treatment resulted in protein structures with high anti-pTDP-43 immunopositivity for both FTLD-TDP-A and FTLD-TDP-C, further confirming that the lack of anti-RRM2 immunogold labeling in FTLD-TDP-C samples (**Fig. 5a**) was due to epitope accessibility within these TDP-43 assemblies. In conclusion, the observed differential resistance to proteolysis indicates distinct aggregate structures in different neuropathological subtypes, in agreement with immunogold-EM analysis.

Differential cyto- and neurotoxicity of FTLD-TDP type A and type C pathological assemblies

In order to determine whether these distinct TDP-43 conformations were associated with different toxic properties, we tested their effect on the viability of cell lines and primary neurons. To this end, we used the Flp-In T-Rex technology to generate a stable cell line with inducible expression of C-terminally tagged TDP-43, to obtain a homogeneous population of cells expressing traceable TDP-43 at similar levels (**Supplementary Fig. 26a-c**), which is unfeasible by transient transfection. We used the HA tag, which comprises of only 9 amino acids and we placed it at the very end of the structurally disordered region to minimize any interference with protein structure, which might hinder protein seeding. We first used our TDP-43-HA-expressing cells to optimize the internalization of SarkoSpin-extracted GFP-labeled pTDP-43 aggregates produced in cells, further demonstrating that our novel extraction method can also be applied to cellular models of disease (**Supplementary Fig. 26d-f**).

To test if SarkoSpin specifically concentrated potentially toxic TDP-43 seeds, we subsequently introduced pellets from six control, nine FTLD-TDP-A and seven FTLD-TDP-C patients into mitotically arrested cells, since the continuous proliferation and high metabolic activity of these cells could mask the toxicity of exogenous aggregates. We reasoned that if toxicity of pTDP-43 assemblies was dependent on seeding of endogenous TDP-43, the effect would be more profound upon increased expression of the substrate, i.e. TDP-43-HA. Therefore, after induction of TDP-43-HA expression with doxycycline, we calculated the ratio of viability between both conditions (+DOX/-DOX). This analysis revealed that upon a 3-fold increase in TDP-43 protein levels (**Supplementary Fig. 26g**), the viability of cells inoculated with FTLD-TDP-A extracts was significantly decreased in comparison to that of cells inoculated with control or FTLD-TDP-C aggregates (**Fig. 6a-b**).

To directly test whether the observed toxicity is dependent on aggregation of endogenous TDP-43 triggered by the exogenous TDP-43 seeds, we subsequently performed SarkoSpin on mitotically arrested TDP-43-HA-expressing cells inoculated with SarkoSpin pellet pools from three control, three FTLD-TDP-A and three FTLD-TDP-C patients. Immunoblot with anti-HA antibody against the

endogenously expressed TDP-43-HA fusion protein allowed for the unambiguous distinction of newly induced aggregates from exogenous patient-derived seeds, Interestingly, while levels of TDP-43-HA were equal in all conditions (**Supplementary Fig. 26g**), cells inoculated with FTLD-TDP-A pellets presented increased TDP-43-HA aggregation, compared to cells treated with control or FTLD-TDP-C seeds (**Fig. 6c**). Collectively, these data indicated that pTDP-43 assemblies extracted from FTLD-TDP-A, but not control or FTLD-TDP-C patients were cytotoxic and induced endogenous TDP-43 aggregation, potentially via protein seeding. These findings are in line with the notion that FTLD-TDP-A aggregate species were more potent, thereby causing a more aggressive clinical phenotype with significantly shorter disease span than FTLD-TDP-C patients (**Supplementary Fig. 1e**).

To confirm the increased potency of FTLD-TDP-A aggregates in a disease-relevant system, we quantified their effect on the neurite length of primary cortical neurons, prepared from E18 mouse embryos and plated in 96-well plates, using high content screening[48]. Neurite length was previously found to be decreased by treatment with artificial oligomers of α-synuclein, which are capable of entering cells and acting as seeds of an autonucleation process[49]. Neuronal cultures were exposed to four different doses of SarkoSpin pellet pools from control, FTLD-TDP-A or FTLD-TDP-C patients (**Fig. 6d**). In order to estimate the protein content of these pellets, all inocula were submitted to immunoblotting against TDP-43, pTDP-43 and actin (**Supplementary Fig. 27**). TDP-43 and pTDP-43 were absent from control SarkoSpin pellets as expected, while their quantity in FTLD-TDP-C inocula was approximately half of FTLD-TDP-A for all doses (**Supplementary Fig. 27a-b**). Importantly, pTDP-43 levels were equivalent between FTLD-TDP-A at dose of 0.3 µg and FTLD-TDP-C at 1 µg total protein, which allowed the direct comparison of the two types of pathological pTDP-43 assemblies. Total protein amounts were normalized against actin for all doses between control, FTLD-TDP-A and FTLD-TDP-C (**Supplementary Fig. 27c**). The effect of exogenous pTDP-43 SarkoSpin extracts on neurite growth was then monitored by automated live cell imaging with combined phase-contrast and epifluorescence imaging over 10 days (**Fig. 6e,f**). In agreement with our observations in immortalized cells, TDP-43 aggregates extracted from FTLD-TDP-A drastically reduced neurite length (**Fig. 6h**),

497 which reached a plateau immediately after inoculation (after 5 days *in vitro* (DIV) at 55 nm length),
498 while control or FTLD-TDP-C SarkoSpin pellets had no effect (plateau reached after 10 DIV at 80 nm
499 neurite length). At 10 DIV, all primary neuronal cultures were submitted to calcein fluorescence
500 imaging allowing counting of cell bodies and measuring neurite length for all conditions (**Fig. 6g-h**). As
501 seen in phase contrast, calcein staining of live cells decreased drastically and proportionally to the
502 dose of FTLD-TDP-A-extracted TDP-43 aggregates, while control and FTLD-TDP-C SarkoSpin pellet
503 inoculations had no effect. This specific neurotoxic effect of FTLD-TDP-A aggregates was measured
504 both by the decrease of cell body number (**Fig. 6g**) and neurite length (**Fig. 6h**) in a dose-dependent
505 manner. Since levels of pTDP-43 in FTLD-TDP-C were identical to those of FTLD-TDP-A at one dose
506 lower (i.e. pTDP-43 levels of FTLD-TDP-C at 0.3 µg dose equals that of FTLD-TDP-A at 0.1 µg dose),
507 indicating that even at equivalent pTDP-43 inoculated amounts, FTLD-TDP-A SarkoSpin pellets
508 inhibited significantly more neurite outgrowth and decreased neuronal viability compared to FTLD-
509 TDP-C ones. Using this approach, automated analysis of the phase contrast and fluorescence images
510 indicated that FTLD-TDP-A extracted TDP-43 pathological aggregates exhibit severe neurotoxicity in
511 a dose-dependent manner (**Fig. 6f-h**).
512 Collectively, our data demonstrate that pathological TDP-43 adopts stable configurations with specific
513 biophysical properties, which allow its physical separation from its physiological counterpart. Notably,
514 the biochemical properties of pathological TDP-43 and a subset of insoluble proteins can discriminate
515 between specific neuropathological subtypes, indicating that they may underlie specific disease
516 characteristics. Most importantly, we show evidence that pTDP-43 aggregates extracted by our new
517 purification method confer cyto-/neurotoxicity accompanied by induced aggregation of endogenous
518 TDP-43. Remarkably, the most toxic aggregates are those found in the brains of FTLD-TDP-A
519 patients, who show significantly shorter disease duration (**Supplementary Fig. 1e**), indicating a direct
520 link between the properties of TDP-43 aggregates and clinical presentation.
521
522 **Discussion**

TDP-43 pathology characterizes most instances of ALS and FTD and its spatiotemporal manifestation coincides with neurodegeneration, supporting its central pathogenic role in these diseases[2]. Despite this unifying TDP-43 pathology, ALS and FTD patients display large heterogeneity in terms of clinical disease presentation, progression and neuropathological findings, a phenomenon that remains mechanistically unexplained. Recent discoveries indicate that several protein aggregation diseases follow a prion-like paradigm[50] through amplification of pathological conformers. These findings provide a plausible explanation of the origin of disease heterogeneity. Indeed, differential quaternary structures of the prion protein are responsible for different subtypes of infectious prion diseases and are associated with distinct neuropathological profiles and clinical presentations[47]. The notion of prion strains was recently expanded to other protein aggregation diseases with compelling data for tau[51], α-synuclein[52] and Aβ,[53], suggesting that this may indeed be a general phenomenon.

Here, we unambiguously show that human patient-derived TDP-43 adopts stable protein assemblies with specific biophysical properties, which allow for its physical separation from its physiological counterpart. We exploited these features to develop a reliable method for the isolation of TDP-43 aggregates from the majority of normal proteins. Following our recent discovery that physiological TDP-43 forms oligomers that bind RNA[11], we combined nuclease-dissociation with detergent solubilization without denaturation to accomplish an unprecedented level of separation of pathological TDP-43 assemblies from physiological complexes. We foresee that our new method, SarkoSpin, will become a valuable tool for any application requiring a source of faithful, disease-associated TDP-43 aggregates.

We used SarkoSpin for the native extraction of pathological TDP-43 from autopsy brain tissues of >80 patients from different types of TDP-43 proteinopathies and controls. An unbiased proteomic approach of isolated pathological assemblies revealed that TDP-43 was the most significantly enriched protein and the only one found insoluble in all disease cases, indicating that we isolated the pTDP-43 core of pathological assemblies. Comparison of other proteins that become insoluble in ALS and FTLD human brains revealed specific subclasses of proteins characterizing each disease

549 subtype. These proteins did not co-localize with pTDP-43 in patient brains and sometimes even
550 occurred in different cell types – i.e. FBXO2 in astrocytes – suggesting that they most likely represent
551 a downstream molecular signature of the divergent pathogenic mechanisms characterizing the
552 different disease subtypes.
553 Combining SarkoSpin with a number of biochemical, molecular and imaging methodologies, we
554 provide evidence that TDP-43 extracted from different disease subtypes exhibits distinct biochemical
555 and morphological features. In particular, the intrinsic density of the isolated particles is remarkably
556 consistent within each disease subtype, while it is a distinguishing feature of pathological TDP-43 in
557 different FTLD types. Our results indicate that FTLD-TDP-C, an exclusively sporadic type of dementia
558 with significantly longer disease duration than other types[29], is associated with very dense TDP-43
559 aggregates showing lower levels of polyubiquitination and a highly protease resistant C-terminal core,
560 compared to TDP-43 assemblies extracted from FTLD-TDP-A or ALS. While no long fibrillary
561 structures were detected within TDP-43 aggregates of either disease subtype, short proteinaceous
562 filaments were present in both, albeit with differential accessibility to specific antibodies, indicative of
563 alternate aggregate packaging. Surprisingly, the neuropathological type, rather than the genetic cause
564 of the disease, better predicted the features of TDP-43 aggregates, indicating that the same genetic
565 trigger may give rise to variable pathological assemblies, perhaps determined by other, still unknown
566 factors.
567 Most importantly, these biochemical and morphological differences in the pTDP-43 assemblies
568 extracted from FTLD-TDP-A or FTLD-TDP-C patients were associated with differential seeding and
569 neurotoxic potential. Indeed, FTLD-TDP-A aggregates caused toxicity and induced endogenous TDP-
570 43 aggregation in cellular models, while FTLD-TDP-C seemed inert under the same conditions and
571 equivalent pTDP-43 doses. This finding indicated that FTLD-TDP-A aggregates extracted from
572 patients with fast progressing disease possessed high seeding and neurotoxic potential, while FTLD-
573 TDP-C aggregates from slow progressing disease were inert Moving forward and following the
574 paradigm now established for several other protein aggregates[51,52,53], it would be exciting to find out

whether these patient-derived TDP-43 pathological conformations can faithfully propagate *in vivo*, reproducing their distinctive features and disease phenotypes in animal models. Collectively, our work suggests that disease heterogeneity may originate from alternate pathological TDP-43 conformations, reminiscent of prion strains and opens new avenues for creating cellular and animal models.

Materials and methods

Cases

Brains were donated to the Queen Square Brain Bank for Neurological disorders, Department of Movement Disorders, UCL Institute of Neurology, London, UK, or the Department of Neurology, University of California, San Diego, CA, USA, or the Netherlands Brain Bank, Netherlands Institute for Neuroscience, Amsterdam, Netherlands (open access: www.brainbank.nl). All patient material has been collected from donors for or from whom a written informed consent for a brain autopsy and the use of the material and clinical information for research purposes has been obtained by the respective institution.

Immunohistochemistry

Fresh tissue from frontal cortex of FTLD-TDP-A cases, either sporadic or with *C9ORF72* mutation, as well as a FTLD-TDP-C cases were fixed with phosphate-buffered 3.65% formaldehyde, embedded in paraffin, cut into 6 µm serial sections and mounted on glass slides. Sections were deparaffinized and rehydrated using a gradient of alcohol. Antigen retrieval was done by boiling the sections in 10 mM citrate buffer (pH 6.0) in a microwave oven. Immunohistochemistry was performed using the avidin-biotin complex (ABC) detection system (Vector Laboratories) and 3,3-diaminobenzidine. Endogenous peroxidases were first quenched with 5% H_2O_2 in methanol for 30 minutes, and sections were blocked in 0.1 mol/L Tris with 2% fetal bovine serum for 5 minutes. Primary antibodies were incubated for 2 hours at room temperature. After washing, sections were sequentially incubated with biotinylated secondary antibodies for 1 hour and avidin-biotin complex for 1 hour. Bound antibody complexes were

visualized by incubating sections in a solution containing 100 mM Tris, pH 7.6, 0.1% Triton X-100, 1.4 mM di-aminobenzidine, 10 mM imidazole, and 8.8 mM H_2O_2. Sections were then lightly counterstained with hematoxylin, dehydrated, and coverslipped. Digital images were obtained using Life Technologies EVOS FL Auto imaging system (Life Technologies).

All antibodies used for immunofluorescence and western blot are listed in **Supplementary Table 2** with the respective catalogue numbers and working dilutions indicated for each assay.

Homogenization of brain tissue

Frozen tissue from motor or frontal cortex of all groups of patients were homogenized at 20 % w/v in homogenization - solubilization buffer (HS) without detergent: 10 mM Tris pH 7.5, 150 mM NaCl, 0.1 mM EDTA, 1 mM DTT, Complete EDTA-free protease inhibitors (Roche) and PhosSTOP phosphatase inhibitors (Roche). Samples were subjected to three rounds of 30 seconds homogenization in tubes containing a mixture of ceramic beads of 1.4 and 2.8 mm of diameter on a Minilys device (Bertin) at full speed with cooling on ice between each round. Samples were aliquoted, snap frozen in liquid nitrogen and kept in -80ºC before use.

SarkoSpin on patient tissues

All SarkoSpin steps were done in 1.5 mL Protein Low Binding tubes (Eppendorf). Brain homogenate aliquots of 150 µL were thawed on ice and equalized for protein concentration in final volume of 200 µL using HS buffer. Samples were then diluted 1:1 in HS buffer with 4% (w/v) N-lauroyl-sarcosine (sarkosyl, Sigma), 2 U/µL Benzonase (Novagen) and 4 mM $MgCl_2$, reaching final volume of 400 µL with 2% Sarkosyl, 1 U/µL Benzonase and 2 mM $MgCl_2$ final concentrations. SarkoSpin solubilization was then performed by incubating at 37ºC under constant shaking at 600 rpm (Thermomixer, Eppendorf) for 45 minutes. Solubilized brain homogenates (400 µL) were then further diluted by adding 200 µL of ice-cold HS buffer containing 0.5% w/v sarkosyl prior to centrifugation at 21,200 g on

a benchtop centrifuge (Eppendorf) for 30 minutes at room temperature. Alternatively, for EM sample preparation, to remove lipids from precipitating along with protein aggregates, solubilized material was overlaid on top of 400 µl sucrose cushion (40% w/v sucrose (Sigma) in HS buffer containing 0.5% w/v sarkosyl) and centrifuged at 21,200 g for 1 hour at room temperature. For the analysis of proteolytic profiles, after the initial 15 minutes of SarkoSpin solubilization, the respective protease was added for the remaining 30 minutes of incubation in the following final concentrations: 100 µg/mL for Proteinase K, 10 µg/mL for Chymotrypsin or 100 µg/mL for Trypsin (from stock solutions of 2 mg/mL, 0.2 mg/mL or 2 mg/mL, respectively). Supernatants (approx. 600 µL) were collected in a new tube and pellets were resuspended in desired volume of HS buffer containing 0.5 % w/v sarkosyl for further analysis, including dot blot, SDS-PAGE and immunoblot or native PAGE. Whenever specified, the fractions were passed through low protein binding 0.22 µm filters (Millex-GV) to remove large non-solubilized particles.

SarkoSpin on cells

Transfected NSC-34 cells in 10 cm dishes (see below) were lysed in 400 µL of ice-cold 1X HS buffer with 0.5% sarkosyl, 2 mM $MgCl_2$ and ~100 U Benzonase, and 60 µL of the lysate was put aside for protein concentration measurements and immunoblots. For SarkoSpin of inoculated HEK cells, cells plated in a 6-well plate were lysed in 170 µl of ice-cold 1X HS buffer with 0.5% sarkosyl, 2 mM $MgCl_2$ and ~25 U Benzonase per well. For sample solubilization, to aliquots of 170 µL of lysate, 52 µL 1X HS and 178 µL 2X HS with 4% sarkosyl were added, for a final concentration of 2% sarkosyl in 400 µL of sample. After a 30-minute incubation on ice with vortexing every 10 minutes, the samples were diluted by adding 200 µL of ice-cold HS buffer and centrifuged as described before for SarkoSpin on brain homogenates. Supernatants were collected in a new tube and pellets were resuspended in 1X HSI buffer with 0.5% sarkosyl for immunoblot samples or in PBS for inoculation experiments in HEK cells. SarkoSpin fractions from cell line experiments were processed for immunoblot as described before for brain homogenates.

Mass Spectrometry

After clean-up with C18 cartridges, the peptide samples were measured on a TripleTOF 5600 instrument (AB Sciex, Concord ON) equipped with a nano-electrospray ion source and an Eksigent 1D-plus liquid chromatography system (Eksigent, Dublin, CA) or a Q Exactive Plus instrument (Thermo Fisher) equipped with an EASY-nLC 1000 (Thermo Fisher). For the TripleTOF measurements, peptides were loaded onto a 20-cm long, 75 µm i.d. PicoFrit Column (New Objective, Woburn, MA) packed in-house with Magic C18 AQ 3 µm beads (Michrom Bioresources, Auburn, CA) and separated with a linear gradient from 5% to 35% acetonitrile in 90 min at a flowrate of 300 nL/min. Survey scans were acquired in 300 ms and up to 20 product ion scans were collected in 75 ms if exceeding a threshold 150 counts per second with a charge state from 2+ to 5+. For the Q Exactive Plus measurements, peptides were loaded on a 40 cm long, 75 µm i.d. column packed in-house with ReproSil-Pur C18-AQ resin (1.9 µm, Dr. Maisch). Peptides were eluted for 50 min using a segmented linear gradient of 5% to 40% acetonitrile at a flow-rate of 300 nL/min. Survey full-scan mass spectra were acquired with mass range 350-1500 m/z, at a resolution of 70,000 at 200 m/z and the 20 most intense ions above an intensity of 3.6e4 were sequentially isolated, fragmented (HCD at 25 NCE) and measured at a resolution of 17,500 at 200 m/z. Peptides with a charge of +1 or with unassigned charge state were excluded from fragmentation for MS2, and a dynamic exclusion of 30 s was applied. Ions were accumulated to a target value of 3e6 for MS1 and of 1e5 for MS2.

MGF-peak lists generated from the acquired spectra by ProteinPilot from the TripleTOF runs and .RAW files from the Q Exactive Plus runs were searched against a human Uniprot protein database (68978 sequence) by Sequest HT in Proteome Discoverer 1.4 (Thermo Scientific, San Jose, CA) with enzymatic specificity trypsin, precursor mass tolerance 20 ppm and fragment tolerance 0.1 Da and 0.02 Da for TripleTOF and Q Exactive Plus, respectively. Methionine oxidation and carbamidomethylation of cysteines were set as respectively variable and static modifications.

Percolator was used to filter the results to a 1% peptide false discovery rate. Spectral counting was used for quantifying protein differences between samples.

Statistical Analysis of Mass Spectrometry Data

Unless stated otherwise the higher-level data analysis was carried out using R/Bioconductor (R Core Team, 2017). The count values for each sample were normalized by dividing the values by the respective trimmed mean (removing the highest and lowest 5% values). As the samples were run in two separate batches, the ComBat method[54] was applied to correct for the batch effect. To identify proteins that were most consistently enriched in patient samples, we established an idealized vector correlation method: a vector of the same number of 0s as control samples and the same number of 1s patient samples was created. For each protein, we measured the correlation of this idealized vector to the vector of normalized and batch-corrected protein abundance values of control and patient samples. We then selected the 50 best-correlated proteins and established a heatmap of the log2 abundance values. For the heatmap, we applied a median per protein normalization, by dividing the values of each protein by the respective median value of the control samples.

Validation of Mass Spectrometry hits by immunofluorescence

Formalin fixed paraffin embedded tissue was sectioned at 7 μm. Sections were deparaffinized in xylene and rehydrated using a gradient of alcohol. Endogenous peroxidases were first quenched with 0.3% H_2O_2 in methanol for 10 minutes. Antigen retrieval was undertaken in a pressure cooker for 10 minutes at maximum pressure in 10 mM citrate buffer (pH 6.0) and sections were blocked in 10% non-fat milk for 30 minutes. Sections were incubated with phosphorylation-specific rabbit polyclonal pAb anti-pTDP (pS409 1:20,000 Cosmobio). After washing, sections were sequentially incubated with biotinylated swine anti-rabbit secondary antibody for 30 minutes and avidin-biotin complex for 30 minutes. pTDP-43 was visualized using TSA Rhodamine amplification (Perkin-Elmer) at 1:500 for 30 minutes. Sections were then incubated with antibodies raised against either TLXN1, FBXO2, ASAH1

followed by incubation in AlexaFluor 468 at 1:1000 for 1 hour at room temperature. Sections were viewed and imaged with a Leica TCS4D using a 3-channel scan head fluorescent microscope and image deconvoluted using Leica software.

Velocity sedimentation and density floatation gradients

Brain homogenates were thawed on ice and solubilized as described previously (SarkoSpin). For velocity sedimentations, a volume of 200 µL was loaded on top of a 4 mL continuous 10-25% iodixanol gradient (Optiprep, Sigma) in HS buffer with 0.5% w/v sarkosyl linearized directly in ultracentrifuge 4.2 mL tubes (Seton) with a Gradient Master (Biocomp). For density floatation gradients, 220 µL of HS buffer with 40% iodixanol and 0.5% w/v sarkosyl was loaded within a 4 mL 10-60% discontinuous iodixanol gradient in HS buffer with 0.5% w/v sarkosyl. The gradients were centrifuged at 310,000 g for 45 min (velocity) or at 125,000 g for 17 hours (density) in a swinging-bucket SW-60 Ti rotor using an Optima XPN-100 ultracentrifuge (Beckman Coulter). Gradients were then segregated into 16 equal fractions from the top using a piston fractionator (Biocomp) and a fraction collector (Gilson). Fractions were aliquoted for further analysis of their content by dot blot, immunoblot on SDS-PAGE or native-PAGE. Gradient linearity was verified by refractometry.

Analysis of protein content of SarkoSpin, velocity and density fractions

Aliquots of the collected fractions were mixed with SDS-PAGE loading buffer with reducing agent (Life Technologies) and denatured at 95ºC for 5 minutes, prior to migration on Bolt 12% Bis-Tris gels (Life Technologies). For visualizing total proteins, gels were stained with silver nitrate. For immunoblots, gels were electro-transferred onto nitrocellulose membranes with iBlot 2 (Life Technologies). For dot blotting, native fractions were spotted onto nitrocellulose 0.2 µm membranes using a dot blot vacuum device (Whatman). Nitrocellulose membranes were blocked with 5 % w/v skimmed powder milk (or 5 % w/v BSA for pS409/410 antibody) in PBS-Tween and probed with primary antibodies (**Supplementary Table 2**). Immunoreactivity was visualized by chemiluminescence (GE Healthcare).

730 The amount of the respective protein in each fraction was determined by the Image Studio Lite
731 software, after acquisition of chemiluminescent signals with a Fuji LAS 4000 digital imager (GE
732 Healthcare). Profiles obtained by immunoblot were normalized and plotted with SD, with all respective
733 student test and ANOVA using the Prism software. Fractions were also subjected to native-PAGE
734 immunoblotting, for which aliquots were mixed with native sample buffer and G250 additive (Life
735 Technologies) and resolved using 3-12% Bis-Tris Native PAGE gels (Life Technologies) and
736 NativeMark protein ladder (Life Techologies). Gels were incubated with 2x transfer buffer and electro-
737 transferred with iBlot 2 on PVDF membranes. After fixation with 8% acetic acid, air-drying and
738 reactivation with methanol, membranes were immunoblotted and probed as described above.
739
740 **Transmission Electron Microscopy**
741 SarkoSpin pellets from different disease types and control patients were resuspended in water and
742 passed through protein low binding 0.22 µm syringe filters. The resulting filtrates were fixed with
743 glutaraldehyde water solution (EMS #16220) (final concentration of 0.05 %) and subjected to immuno-
744 gold labeling. A 300 mesh copper grid (Plano #G2300C), formvar coated and glow discharged, was
745 put on a 3 µL drop of fixed sample for 3 minutes. The grid was then washed 3 times 20 seconds in
746 aldehyde blocking solution with 0.15 % Glycine (Sigma #G7126) in PBS and 3 times 20 seconds in
747 PBS, followed by 5 minute incubation in blocking solution (PBG): PBS with 0.2 % gelatin (Sigma
748 #G6650) and 0.5 % BSA (Applichem #A6588). The grid was probed with TDP-43 60019-2-Ig (mouse
749 1:50 in PBG solution, Proteintech) for 20 minutes (the negative control without primary antibody was
750 incubated instead in PBG solution). The grid was washed in PBG solution 3 times 20 seconds, and
751 incubated for another 5 minutes in PBG, before probing with secondary antibody anti-mouse gold 12
752 nm gold (1:20 in PBG solution, Jackson ImmunoResearch #115-205-146) for 20 minutes. The grid
753 was washed 4 times 20 seconds in PBG and twice 20 seconds in PBS, followed by a second fixation
754 step for 30 seconds in 0.1 % glutaraldehyde in PBS and 4 times 20 seconds washed in water. The
755 grid was then counterstained with 1 % uranyl acetate (Fluka #73943) in water for 1 minute. Excess

solution was sucked off using filter paper and the grid was air-dried. Alternatively, to avoid drying artifacts, the counterstaining solution included 1.8 % methylcellulose (Sigma) in water and 0.3 % uranyl acetate in water (incubation for 3 minutes staining procedure on ice). Lastly, the grid was picked up with a loop, excess solution was sucked off with filter paper, air-dried, and the specimen imaged with a CM100 transmission electron microscope (Thermo Fisher Scientific, Eindhoven, The Netherlands) at an acceleration voltage of 80 kV using a Gatan Orius 1000 digital camera (Gatan, Munich, Germany).

Plasmid generation

A multiply-tagged TDP-43-encoding pcDNA5 plasmid[55] was modified in order to obtain a sequence coding for a single C-terminally HA-tagged TDP-43. The N-terminal GFP, His6 and myc (2) tags and the residual C-terminal amino acids between the HA tag and the stop codon were deleted in two subsequent reactions using the Q5 Site-Directed Mutagenesis Kit (New England Biolabs, E0554S) according to the manufacturer's instructions, with the following primers: 5'-TCT GAA TAT ATT CGG GTA ACC GAA GAT GAG AAC GAT GAG-3', 5'- CAT CCG CGG GGC AGG GGT-3' (tags, Ta = 72 ºC), 5'-TAA ACC CGC TGA TCA GCC-3', 5'-AGC ATA ATC AGG GAC ATC ATA AG-3' (residual amino acids, Ta = 63 ºC).

Cell culture, stable cell line generation and transient transfection

HEK293 Flp-In T-REx cells (Invitrogen, R78007) were cultured in DMEM (Sigma, D5671) supplemented with 10% FBS (Gibco, 10270-106), 1X PenStrep (Gibco, 15140-122), 1X GlutaMAX (Gibco, 35050061), 15 µg/mL blasticidin S (Gibco, R21001; Invivogen, ant-bl-10p) and 100 µg/mL zeocin (Gibco, R25001). In order to generate a stable cell line expressing HA-tagged TDP-43, $3 \cdot 10^5$ cells were plated per well in a 6-well plate and transfected after 48 hours with 125 ng of pcDNA5-TDP43-HA plasmid and 1125 ng of pOG44 plasmid with 6.25 µL Lipofectamine 2000 (Invitrogen, 11668019) according to the manufacturer's instructions. After a 48-hour recovery, cells were

passaged to a 10-cm dish with same media as before with the substitution of zeocin for 100 µg/mL hygromycin (Gibco, 10687-010) for the selection of cells that integrated the TDP-43-HA encoding sequence in the genome. Cells were selected for 2-3 weeks before expansion and banking, and afterwards cultured in the same medium.

For production of SarkoSpin-insoluble phosphorylated GFP-TDP-43 aggregates, $2 \cdot 10^6$ motor neuron-like mouse NSC-34 cells were plated on a Matrigel-coated (Corning, 354234) 10 cm dish in differentiation media, consisting of DNEM/F-12 (Gibco, 21331-020) supplemented with 1X B27 supplement (Gibco, 17504-044), 1% GlutaMAX, 1X N2 supplement (Gibco, 175020-01) and 0.1X PenStrep. After 48 hours, cells were transfected with 5 µg of GFP-TDP-43-HA and 20 µL Lipofectamine 2000 according to the manufacturer's instructions.

Viability assay on HEK293 cells

To study the toxicity of the SarkoSpin-insoluble pellets, $6 \cdot 10^4$ HEK293 cells/well were plated on a Matrigel-coated 24-well plate and TDP-43-HA expression was induced after 24 hours with 1 µg/mL of doxycycline. 20 hours later, cells were mitotically arrested with 10 µM AraC (Sigma, C1768), and after another 6-8 hours, transfected with freshly-prepared SarkoSpin pellet fractions. To prepare the inocula, SarkoSpin pellets were washed with 300 µl of sterile PBS to remove traces of sarkosyl and remove the vast majority of lipid contaminants. Pellets were subsequently resuspended in 200 µl cell-culture grade PBS and sonicated at 60% amplitude for 2 minutes of sonication time (1 s ON /1 s OFF pulses) in water-bath sonicator (Q500, QSonica). 20 µl of sonicated material was transfected with 2.5 µL Lipofectamine in a total volume of 290 µL OptiMEM per well. Additional 210 µL of media was added 4 hours after protein transfection, followed by whole media change after 24 hours, with fresh doxycycline and AraC. For the viability measurements, on day 3 after lipofection, 55 µL of 5 mg/mL Thiazolyl Blue Tetrazolium Bromide (Sigma, D5655) was added per well and incubated at 37 ºC for 1 hour. The reaction was stopped and the formazan solubilized with 100 µL of a solution containing 16% sodium dodecyl sulfate (SDS), 40% dimethylformamide (DMF) and 2% glacial acetic acid.

Absorption of the solubilized formazan at 570 nm was subtracted the absorption from cell debris and other contaminants at 630 nm. The values of absorption in cells expressing TDP-43-HA were divided by the those of non-induced cells, and the value of the ratio of cells inoculated with SarkoSpin pellets from control patients set to one by dividing every value by the average ratio of all control conditions. Every condition was performed in triplicates.

Immunocytochemistry

TDP-43-HA-expressing HEK293 on microscopy 24-well plates (Ibidi, 82406) inoculated with GFP-TDP-43-HA aggregates were wash once with PBS before fixation in 4% formaldehyde (brand) for 10 minutes at room temperature. After washing twice with PBS, cells were permeabilized and blocked in blocking buffer (10% donkey serum (Millipore) with 0.3% Triton X-100 (Sigma) in PBS) for at least 30 minutes at room temperature. Primary antibodies against HA-tag (1:500, Cell Signalling Technologies) and GFP (1:1000, Rockland Immunochemicals) were incubated in blocking buffer overnight at 4 ºC. After three washes with PBS, secondary antibody Alexa-647 donkey anti-rabbit (Invitrogen, A-31573) was applied in PBS for 1 hour at room temperature, followed by three additional washes in PBS. Cells were covered with coverslips using ProLong Gold Antifade Mountant with DAPI (Invitrogen, P36931).

Primary mouse cortical neuronal culture in 96-well plate

Timed pregnant C57/BL6J female mice were received from Charles River Labs 2 days before initiation of the primary culture. Cortices were harvested from E18 mouse embryos and dissociated enzymatically and mechanically (using the neuronal tissue dissociation kit, C-Tubes, and an Octodissociator with heaters, Miltenyi Biotech, Germany) to yield a homogenous cell suspension. The cells were then plated at 20000 per well in 96-well plates in neuronal medium (Neuronal Macs medium, Miltenyi Biotech, Germany) containing 0.5% Penicillin/Streptomycin, 0.5 mM alanyl-glutamine, and 2% Neurobrew supplement (Miltenyi Biotech, Germany). In such cultures, and in control conditions, neurons represented approximately 85-95% of the cell population, with astrocytes

and oligodendrocytes reaching 5-15% (GFAP+ or CNPase+), while the microglia (Iba1+) were undetectable (not shown). Thus, in the text, and for the sake of simplicity, they are referred to as "neurons". After 4 days *in vitro* (DIV), Sarkospin pellet pools from 3 Control, 3 FTLD-TDP-A or 3 FTLD-TDP-C patients were resuspended in sterile PBS and sonicated with a cup horn sonicator (Q500, QSonica) at 100% set amplitude for 4 minutes of 1 second pulse / 1 second pause, and added to the medium at four different dilutions after normalization based on BCA-measured protein concentrations (1, 0.3, 0.1, 0.03 µg of total protein amount). For controlling total protein amounts, as well as levels of TDP-43 and pTDP-43 in the inocula, all treatment medium were submitted to dot blotting with antibodies against actin, TDP-43 and pTDP-43.

High content imaging of neurite outgrowth

Neuritic network development was followed by phase contrast[48]. The signal was acquired using an Incucyte S3 platform (Essen Biosciences) with a 20x objective. White light was used for phase contrast, green and red leds for fluorescence. Neurite outgrowth was computed from both the phase contrast (time lapse) and fluorescence images (endpoint) using the Neurotrack software (Essen Biosciences). At 4 DIV, cultures were then challenged with the four concentrations of SarkoSpin pellets or medium for untreated wells. At 6 days post inoculations, effects of the treatments were evaluated by live cell staining with Calcein-AM to visualize the viable neurons and their processes.

Figure legends (max 250 words/legend)

Figure 1: SarkoSpin physically separates pathological TDP-43 from the majority of normal proteins in FTLD and ALS brains

a. Schematic representation of SarkoSpin protocol, including the number of autopsy samples from each disease type used in this figure. Briefly, samples were homogenized and solubilized with sarkosyl at 37°C in presence of Benzonase prior to a single centrifugation step to separate

supernatant and pellet fractions. **b-j.** Biochemical analysis of SarkoSpin fractions extracted from human brain samples. Supernatants and pellets were subjected to SDS-PAGE followed by silver staining of total protein (**c**), or immunoblotted against total TDP-43 (**b**, **e**), phosphorylated TDP-43 at position S409/410 (pTDP-43) (**g**), or hnRNPA1, hnRNPH, FUS, SOD1, Histone H3 and actin antibodies (**i**). Physiological TDP-43 was found exclusively in supernatants for all patients, while the pathological species marked by phosphorylation were pelleted for all disease types, but are absent in controls. Pathological posttranslational modifications (PTMs) of TDP-43 were observed specifically in SarkoSpin pellets of disease cases: poly-ubiquitination smear (***), hyper-phosphorylation of TDP-43 detected by both anti-pTDP-43 (S409/410) and anti-TDP-43 (total) as a slower migrating band at 45 kDa (**) and the C-terminal fragment of 25 kDa (*). **d,f,h,j.** Quantifications of the percentage of each protein residing in SarkoSpin supernatant or pellet for all patients used in this experiment. Error bars represent standard deviations. S – supernatant, P – pellet.

Figure 2: SarkoSpin extracts from different disease subtypes have distinct protein compositions beyond TDP-43

a. Overlap of proteins with the highest values of idealized vector correlation when comparing each ALS, FTLD-TDP-A, and FTLD-TDP-C to controls. Only proteins with strong correlation values >0.5 were taken into account. The only common protein among the three disease subtypes is TDP-43. The proteins of interest, which were further validated by immunoblot and immunohistochemistry analysis of the SarkoSpin pellets, are highlighted in bold. **b.** Representative immunoblots on SarkoSpin pellet probed against several mass spectrometry hits – PFN1, ASAH1 and TXNL1, showing their enrichment in the insoluble fraction in respective disease subtypes. **c.** Correlation dot plots of pTDP-43 levels and insolubility of selected mass spectrometry candidates analyzed in (**b**).. **d.** Representative immunoblots on SarkoSpin pellet and supernatant fractions probed with ubiquitin antibody, indicating enrichment of ubiquitinated pathological assemblies in the SarkoSpin pellets fractions. **e.** Correlation dot plot of pTDP-43 and ubiquitin levels in SarkoSpin pellets across disease

subtypes. **f.** Co-immunofluorescence of pTDP-43 with ubiquitin in FTLD-TDP-A and FTLD-TDP-C post mortem brain sections. **g.** Quantification of aggregates double-positive for pTDP-43 and ubiquitin in FTLD-TDP-A and FTLD-TDP-C, showing significantly lower ubiquitination levels in type C (dots represent single % values quantified per each image; the error bars show mean with SD). **h.** Representative images of co-immunofluorescence of GFAP marking astrocytes with a mass spectrometry hit FBXO1, showing its upregulation in astroglia specifically in FTLD-TDP-A, but not FTLD-TDP-C. In panels **f** and **h** the images are overlaid with DAPI nuclear staining in blue.

Figure 3: Diverse size distributions of TDP-43 aggregates isolated from different types of TDP-43 proteinopathies

a. Schematic representation of the velocity sedimentation protocol. After SarkoSpin solubilization, brain homogenates were loaded on top of iodixanol gradients and fractionated by sedimentation velocity upon ultracentrifugation. **b.** Representative immunoblots of the distribution of TDP-43 (top panels, immunoblots) and pTDP-43 (lower panels, dot blots) on velocity sedimentation fractions (numbered from top to bottom of the gradient). **c-d.** The relative amounts of TDP-43 (**c**), and pTDP-43 (**d**) per fraction were quantified from control (black, n=6), ALS (red, n=4), FTLD-TDP A (green, n=10), FTLD-TDP C (blue, n=8) velocity sedimentation fractionations. Data presented are the mean curves (bold lines) with standard deviations (lighter shade areas) for each patient group. Panels below the graphs show the statistical significance of the difference in TDP-43 partition in each fraction, based on student t-test comparisons of the different groups.

Figure 4: Distinct density profiles of TDP-43 aggregates isolated from different types of TDP-43 proteinopathies

a. Schematic representation of the density floatation protocol. Briefly, after SarkoSpin solubilization, brain homogenates were loaded in the middle of iodixanol gradients and fractionated by density upon isopycnic equilibrium ultracentrifugation. **b.** Representative immunoblots of the density sedimentation

profiles of physiological and pathological TDP-43 in various disease types. SarkoSpin-solubilized brain homogenates from frontal and motor cortex of control (black), ALS (red), FTLD-TDP-A (green), and FTLD-TDP-C (blue) were fractionated by density and the distribution of total TDP-43 (top panels, immunoblots) and of pTDP-43 (bottom panels, dot blots) was analyzed in the collected fractions (numbered from top to bottom of the gradient). Density values calculated by refractometry are indicated on the top of the graph. **c-d.** The relative amounts of TDP-43 (**c**), and pTDP-43 (**d**) per fraction were quantified from all immunoblots of control (black, n=6), ALS (red, n=4), FTLD-TDP-A (green, n=10), FTLD-TDP-C (blue, n=8) density fractionations. Data presented are the mean curves (bold lines), with standard deviations (lighter shade areas) for each group of patients. Panels below the graphs show the statistical significance of the difference in TDP-43 partition in each fraction, based on student t-test comparisons of the different groups.

Figure 5: Distinct structure of pathological TDP-43 isolated from different disease subtypes

a. Transmission Electron Microscopy (TEM) images of SarkoSpin-extracted aggregates from control (black frame), FTLD-TDP type A (green frame) and FTLD-TDP type C (blue frame) immunolabeled with monoclonal TDP-43 antibody (epitope: 203-209). All the EM grid samples were embedded in methylcellulose to avoid drying artifacts. The red arrows point to examples of gold-positive structures, while the yellow arrows point to lipid contaminants, which are pulled down in SarkoSpin together with the pathological protein assemblies. The orange arrows to proteinaceous filamentous structures. **b.** To better visualize these filamentous structures**,** part of the FTLD-TDP-C image shown in panel **a** was band-pass filtered. The scale bar is 100 nm **c.** TEM images of SarkoSpin-extracted aggregates from FTLD-TDP-A patient immunogold labeled against TDP-43, without the additional step of embedding in methylcellulose (MC), in order to obtain higher imaging resolution. In panels **a** and **b**. **c.** Proteolytic profiles of pathological TDP-43 from different disease subtypes, as annotated. Two control and four of each ALS, FTLD-TDP-A and FTLD-TDP-C samples were incubated with either 10 µg/mL Chymotrypsin (upper blots) or 100 µg/mL Trypsin for 30 min at 37^{o}C during SarkoSpin solubilization.

Pellets were immunoblotted with anti-TDP-43 antibodies, raised against defined protein regions, showing distinct proteolytic fragments for each disease group. As a reference to the antigens and epitopes of used antibodies, TDP-43 secondary structure is represented below. NTD – N-terminal domain; NLS – nuclear localization signal; RRM1 and 2 – RNA-recognition motifs; LCD – low-complexity domain; Phosphorylation is marked by added phospho-groups at the very C-terminus of TDP-43. **d.** Dot plot representing the levels of pTDP-43 Chymotrypsin and Trypsin-resistant fragments normalized to total level of undigested TDP-43 species across disease subtypes, showing significantly higher Trypsin-resistance of aggregates extracted from FTLD-TDP-C or ALS compared to the ones in FTLD-TDP-A (dots represent single analyzed patients per disease subtype; the error bars show mean with SD). **e.** Representative TEM images of trypsinized SarkoSpin-extracted aggregates from FTLD-TDP type A and type C immunogold-labeled against pTDP-43 pS409/410. Red arrows point to examples of gold-positive structures.

Figure 6: Differential cyto- and neurotoxicity of FTLD-TDP type A and type C pathological assemblies **a.** Schematic representation of SarkoSpin inoculations on arrested HEK293 cells expressing TDP-43-HA. Briefly, expression of TDP-43-HA was induced with doxycycline 24hrs after plating the cells and their growth was arrested with AraC before lipofection of SarkoSpin pellets from control (n=6), FTLD-TDP-A (n=9) and FTLD-TDP-C (n=7) postmortem brain samples. At 3 days after inoculation, viability was measured by MTT assay or cells were collected for SarkoSpin analysis. **b.** Viability ratio of cells inoculated with SarkoSpin pellets from different patients with induced expression of TDP-43-HA (+DOX) and without it (-DOX). Each point represents the viability ratio of cells inoculated with the SarkoSpin pellet of a single patient; bars show mean ± SD. **c.** Immunoblots of SarkoSpin supernatant and pellet fractions from TDP-43-HA-expressing cells inoculated with SarkoSpin pellet pools extracted from control (n=3), FTLD-TDP-A (n=3) or FTLD-TDP-C (n=3) patients. Full-size blots are shown in **Supplementary Fig. 26h**. **d.** Schematic representation of neurite outgrowth and toxicity assay on mouse primary cortical neuronal cultures upon inoculations of SarkoSpin pellets from different disease

subtypes. Briefly, cortical neurons from E18 mouse embryos were dissociated and plated in 96-well plates, challenged at 4 DIV with SarkoSpin pellet pools extracted from control (n=3), FTLD-TDP-A (n=3) and FTLD-TDP-C (n=3) patients and monitored for neurite outgrowth by phase contrast and fluorescence using an IncuCyte S3. **e.** Representative fluorescence calcein (green, upper rows) images and corresponding neurite and cell body segments (blue and yellow respectively, lower rows) for control (upper panel), FTLD-TDP-A (middle panel) and FTLD-TDP-C (lower panel) SarkoSpin pellet inoculations at indicated total protein amounts at 10 DIV endpoint. **f.** Dynamics of neurite outgrowth revealed by quantification of the phase contrast images for control (black), FTLD-TDP-A (green) and FTLD-TDP-C (blue) SarkoSpin pellets inoculated neurons at 0.3 µg total protein dose per well. **g.** Quantification of the endpoint calcein fluorescence images using a cell body segmentation algorithm for different doses of SarkoSpin extracts derived from control (black), FTLD-TDP-A (green) and FTLD-TDP-C (blue). **h.** Quantification of the endpoint calcein fluorescence images using a cell body segmentation algorithm for different doses of SarkoSpin extracts derived from control (black), FTLD-TDP-A (green) and FTLD-TDP-C (blue). Both **g** and **h** confirm the dose response of FTLD-TDP-A aggregates visually apparent in **e**.

Supplementary Figure Legends

Supplementary Table 1: Summary of patient information of the autopsy material used in this study

Summary table of the different groups of patient autopsy material used in this study, with number of patients and identified genetic causes. All samples were used for development and standardization of the SarkoSpin method. FTLD: Frontotemporal Lobar Degeneration. ALS: Amyotrophic Lateral Sclerosis. FTLD-TDP: FTLD with TDP-43 pathology. FTLD-Tau: FTLD with Tau pathology. Sporadic: No identified genetic cause and absence of familial history. *C9ORF72*: Hexanucleotide repeat expansions in chromosome 9 open reading frame 72. *GRN*: Granulin mutation. *MAPT*: Microtubule-Associated Protein Tau mutation.

Supplementary Figure 1: Characteristics of disease subtypes and correlation to disease duration

a. Phosphorylated TDP-43 immunohistochemical staining of temporal cortex from FTLD-TDP subtypes, highlighting differences in their pathological hallmarks. Neuronal cytoplasmic inclusions (NCI) (arrows) and short dystrophic neurites (DN) (arrowhead) were observed in FTLD-TDP-A without (toppanel) or with (middle panel) *C9ORF72* repeat expansions. In FTLD-TDP-C, long twisted neurites were observed (lower panel, arrowhead). Scale bar 25 μm. **b-c.** Age at death (**b**) and disease duration (**c**) of patients from the different disease groups used in the study. FTLD-TDP-C patients showed significantly longer disease duration.

Supplementary Figure 2: Benzonase treatment releases physiological TDP-43 complexes from SarkoSpin pellets

a. Schematic representation of sequential insolubility assay. Brain homogenates are solubilized with indicated detergents (without Benzonase) and centrifuged after each solubilization step. Each time, pellets are resuspended in buffer with increasing detergent stringency until the SDS-insoluble fraction. **b.** Sequential insolubility fractions from control (black, left panels) and ALS (red, right panels) were subjected to SDS-PAGE followed by immunolabeling of TDP-43 (top) and hnRNP A1 (bottom). Both of these proteins are present in SDS fraction, in any health or disease case, showing the importance of using Benzonase for assessing the insolubility of nucleic acid binding proteins. **c.** Biochemical analysis of sarkosyl-soluble and insoluble fractions extracted from human brain samples, with or without Benzonase treatment as noted. Supernatants and pellets were subjected to SDS-PAGE followed by silver staining of total protein (upper panel), or immunoblotted against total TDP-43 (middle panel) or phosphorylated at position S409/410 TDP-43 (pTDP-43) (lower panel). Physiological TDP-43 in the pellet of the control sample (black arrow) is released upon Benzonase treatment (white arrow).

Supplementary Figure 3: Immunoblots of SarkoSpin fractions from all groups of patients show consistent isolation of pTDP-43

Brain from control (black, C), ALS (red), FTLD-TDP type A (green, F-A), type B (yellow, F-B) and type C (blue, F-C) motor cortex (**a, b**) and frontal cortex (**c**) were subjected to SarkoSpin. The supernatant and pellet fractions were analyzed by SDS-PAGE and immunoblotted against TDP-43, pTDP-43, hnRNPA1 and SOD1 antibodies. Posttranslational modifications related to pathological TDP-43 are marked with asterisks: poly-ubiquitination smear (***), hyper-phosphorylation (**) and C-terminal fragmentation (*). S- supernatant, P – pellet, L – ladder.

Supplementary Figure 4: Immunoblots against TDP-43 with different mono- and polyclonal antibodies

Total homogenates from frontal and motor cortex of control (black), ALS (red), FTLD-TDP A (green), B (yellow) or C (blue) were subjected to SDS-PAGE after equilibration of protein amounts, and were immunoblotted with monoclonal (two left panels), polyclonal (two right panels) anti-TDP-43 or actin antibodies. The monoclonal 60019-2-Ig antibody detected an additional unspecific band just below 40 kDa. This band is not observed with any other anti-TDP-43 antibody used.

Supplementary Figure 5: Estimated percentages of pathological and physiological TDP-43 assemblies in human brain

a. Percentages of phosphorylated TDP-43 in control and patient brain SarkoSpin preparations were calculated considering that only phosphorylated TDP-43 is present in SarkoSpin pellets, and knowing the fraction of total TDP-43 in this pellet. Each dot represents a value from a single patient and the line is the average for each group. **b.** Calculated percentages of aggregated TDP-43 from velocity sedimentations. The sum of relative amount of TDP-43 in fractions 6 to 16 (aggregated TDP-43) of velocity sedimentations from control (black, n=6), ALS (red, n=4), FTLD-TDP-A (green, n=7), and FTLD-TDP-C (blue, n=7) was divided by the sum of relative amount in fractions 1 to 5 (normal TDP-

43) in order to estimate the ratios between these two forms of the protein, which are represented as a percentage of the total. Each dot represents a value from a single patient and the line is the average for each group. **c.** Percentage of oligomeric TDP-43 was estimated in control samples, based on Native PAGE TDP-43 immunoblots, where oligomeric TDP-43 appears in fractions 5 to 7 as a broad smear, while monomeric TDP-43 concentrates in fractions 8-12 as a condensed band of apparent ~66 kDa. Each dot represents a value from a single patient and the line is the average.

Supplementary Figure 6: SarkoSpin captures native pathological TDP-43 assemblies

Native PAGE immunoblots of SarkoSpin supernatants (top panels) and pellets (lower panels) extracted from different disease types were immunoblotted against total TDP-43 (left panels) or pTDP-43 (pS409/410, right panels). The indicative molecular weights were established by NativeMark protein ladder, and material retained in the stacking gels was considered of more than 10 MDa.

Supplementary Figure 7: SarkoSpin extracts from different ALS and FTLD samples have distinct protein compositions beyond TDP-43

Abundance levels of selected proteins that were most consistently different in patient samples of human TDP-43 proteinopathies, FTLD-Tau (FTLD-T) and controls. We applied the idealized vector method for control and pooled TDP-43 proteinopathy samples (ALS, FTLD-TDP-A, FTLD-TDP-B and FTLD-TDP-C). The top 50 correlating proteins were sorted based on these correlation values, which are shown bar plot on the right. Strong correlation values ($r > 0.5$) were separated from medium and weak correlation values by the red dashed line.

Supplementary Figure 8: Proteins enriched in SarkoSpin pellets of ALS brains

Abundance levels of selected proteins that were most consistently different in ALS brain samples compared to controls. We applied the idealized vector method for control and ALS samples. The top 50 correlating proteins were sorted based on these correlation values, which are given as a bar plot

on the right. Strong correlation values (r >0.5) were separated from medium and weak correlation values by the red dashed line.

Supplementary Figure 9: Proteins enriched in SarkoSpin pellets of FTLD-TDP-A brains

Abundance levels of selected proteins that were most consistently different in FTLD-TDP-A brain samples compared to controls. We applied the idealized vector method for control and FTLD-TDP-A samples. The top 50 correlating proteins were sorted based on these correlation values, which are given as a bar plot on the right. Strong correlation values (r > 0.5) were separated from medium and weak correlation values by the red dashed line.

Supplementary Figure 10: Proteins enriched in SarkoSpin pellets of FTLD-TDP-B brains

Abundance levels of selected proteins that were most consistently different in FTLD-TDP-B brain samples compared to controls. We applied the idealized vector method for control and FTLD-TDP-B samples. The top 50 correlating proteins were sorted based on these correlation values, which are given as a bar plot on the right. Strong correlation values (r > 0.5) were separated from medium and weak correlation values by the red dashed line.

Supplementary Figure 11: Proteins enriched in SarkoSpin pellets of FTLD-TDP-C brains

Abundance levels of selected proteins that were most consistently different in FTLD-TDP-C brain samples compared to controls. We applied the idealized vector method for control and FTLD-TDP-C samples. The top 50 correlating proteins were sorted based on these correlation values, which are given as a bar plot on the right. Strong correlation values (r > 0.5) were separated from medium and weak correlation values by the red dashed line.

Supplementary Figure 12: Further characterization on the protein content in SarkoSpin soluble and insoluble fractions in different neuropathological subtypes

a. Representative immunoblots on SarkoSpin soluble fractions corresponding to immunoblots on insoluble material in **Fig. 2b**. **b.** Full-size immunoblots on SarkoSpin supernatant and pellet fractions probed against PFN1, showing unspecific bands above 30 kDa (**) in addition to the specific Profilin band at 15 kDa (*). **c.** Immunoblot on SarkoSpin pellets probed against total TDP-43 **d.** Correlation dot plot of pTDP-43 and total TDP-43 quantified from (**c**). **e.** Representative co-immunofluorescence of pTDP-43 and ubiquitin in control, FTLD-TDP-A and FTLD-TDP-C brain sections corresponding to merged images in **Fig. 2f**.

Supplementary Figure 13: Co-immunofluorescence of pTDP-43 with mass spectrometry hits, ASAH1 and TXNL1

Representative images of co-immunofluorescence of pTDP-43 with selected mass spectrometry hits ASAH1 (**a**) and TXNL1 (**b**) in control, FTLD-TDP-A and FTLD-TDP-C post mortem brain sections. On the right side, high magnification images are shown, with examples of partial co-localization of pathological pTDP-43 aggregates with ASAH (1) and TXNL1 (2) in FTLD-TDP-A and with TXNL1 (3) in FTLD-TDP-C. All images are overlaid with DAPI nuclear staining in blue.

Supplementary Figure 14: FBXO1 upregulation in astrocytes in FTLD-TDP-A patients, but not FTLD-TDP-C

a. Representative immunohistochemistry images showing FBXO1 immunoreactivity in control, FTLD-TDP-A and FTLD-TDP-C brain sections. **b**. Representative co-immunofluorescence of GFAP and FBXO1 in control, FTLD-TDP-A and FTLD-TDP-C brain sections corresponding to merged images in **Fig. 2h**. All images are overlaid with DAPI nuclear staining in blue.

Supplementary Figure 15: Distinct size distributions of TDP-43 aggregates isolated from different types of TDP-43 proteinopathies

Brain homogenates from control (black, n=6), FTLD-Tau (grey, n=2), ALS (red, n=4), FTLD-TDP-A (green, n=11), FTLD-TDP-B (yellow, n=3) and FTLD-TDP-C (blue, n=9) patients were subjected to SarkoSpin solubilization and velocity sedimentation by ultracentrifugation on a continuous iodixanol gradient. The collected fractions (numbered from top to bottom of the gradient) were analyzed for TDP-43 (left panel) and pTDP-43 (right panel) content by dot blot.

Supplementary Figure 16: Immunoblots representing the distribution of TDP-43 and pTDP-43 on velocity sedimentation gradients

a-b. Representative immunoblots of the velocity sedimentation profiles of TDP-43 (**a**) and pTDP-43 (**b**). SarkoSpin solubilized brain homogenates from frontal and motor cortex of control (black), FTLD-TDP-A (green), and FTLD-TDP-C (blue), were fractionated by velocity and the collected fractions (numbered from top to bottom of the gradient) were analyzed for TDP-43 (**a**) and pTDP-43 (**b**) by western blotting.

Supplementary Figure 17: Neuropathological profile rather than genotype correlates with the size distribution of pathological TDP-43

a-b. Relative distribution of TDP-43 and pTDP-43 (lower graph) on sedimentation velocity fractionations of FTLD-TDP type A (green) and B (yellow) patient brain samples. SarkoSpin solubilized brain homogenates from frontal and motor cortex of sporadic, *GRN* and C9ORF72 patient brain samples were fractionated by velocity. The relative amounts of TDP-43 (**a**), and pTDP-43 (**b**) per fraction were quantified from immunoblots. Data presented are the mean curves (bold lines) with standard deviations (lighter shade areas) for each group of patients. Panels below the graphs show the statistical significance of the difference in TDP-43 partition in each fraction, based on student t-test comparisons of the different groups.

Supplementary Figure 18: Velocity sedimentation and density floatation profiles of human recombinant TDP-43 aggregated *in vitro*

Representative silver stainings of the distribution of human recombinant full-length TDP-43, aggregates reconstituted *in vitro* on velocity sedimentation (**a**) and density floatation (**c**) gradients. TDP-43 velocity (**b**) and density (**d**) profiles of recombinant TDP-43 aggregates are represented as the mean curves (bold lines), with standard deviations (lighter shade areas). **d.** Representative native PAGE silver staining of recombinant TDP-43 fractionated by density. Only fractions 1 to 14 were loaded due to available wells on native PAGE gels. Note the presence of high molecular weight assemblies retained in the stacking gel (increased exposure on top panel).

Supplementary Figure 19: Sedimentation profiles of FUS, SOD1 and hnRNPA1 in human brains

Representative immunoblots of the distribution of FUS, hnRNPA1 and SOD1 on velocity sedimentation gradients. SarkoSpin-solubilized brain homogenates from frontal and motor cortex of control (black), ALS (red), FTLD-TDP-A (green), and FTLD-TDP-C (blue) were fractionated by velocity and the collected fractions (numbered from top to bottom of the gradient) were analyzed for FUS (top), hnRNPA1 (middle) and SOD1 (bottom) content by western blotting.

Supplementary Figure 20: Distinct density profiles of TDP-43 aggregates isolated from different types of TDP-43 proteinopathies

SarkoSpin-solubilized brain homogenates from control (black, n=6), FTLD-Tau (grey, n=2), ALS (red, n=4), FTLD-TDP type A (green, n=11), B (yellow, n=3) and C (blue, n=9) patients were fractionated by density upon isopycnic equilibrium floatation gradients. The collected fractions (numbered from top to bottom of the gradient) were analyzed for TDP-43 (**a**) and pTDP-43 (**b**) content by dot blot. The density values calculated by refractometry are indicated on the top of the gradients.

Supplementary Figure 21: Immunoblots representing the distribution of TDP-43 and pTDP-43 on density floatation

a-b. Representative immunoblots of the distribution of TDP-43 (**a**) and pTDP-43 (**b**) on velocity gradients. SarkoSpin-solubilized brain homogenates from frontal and motor cortex of control (black), FTLD-TDP-A (green), and FTLD-TDP-C (blue) were fractionated by density and the collected fractions (numbered from top to bottom of the gradient) were analyzed for pTDP-43 and TDP-43 content by western blotting.

Supplementary Figure 22: Density estimation and linearity of iodixanol gradient fractions

a. Fractions of density floatation gradients were loaded on an optical refractometer (Zeiss). Their density was calculated from tables of correlations between refractive index (RI density) or iodixanol concentration (% iodixanol density) and density, respectively, provided by the Optiprep medium manufacturer. The average density of each fraction was determined as a mean of the measured and calculated densities. **b.** The linearity of density in iodixanol gradients was assessed by plotting the average of measured and calculated density of each fraction as described above, with a linear correlation R^2 of 0.99964.

Supplementary Figure 23: Verification of the size of TDP-43 aggregates segregated by density floatation gradients

Representative Native PAGE immunoblots of TDP-43 (left panels), and pTDP-43 (right panels) on density fractionations from control (black), FTLD-TDP-A (green), and FTLD-TDP-C (blue) patient brain samples. Only fractions 1 to 14 were loaded due to available wells on native PAGE gels. Density values calculated by refractometry are indicated on the top of the graph. pTDP-43-positive pathological aggregates are seen at >10 MDa for FTLD-TDP-A and FTLD-TDP-C (green and blue arrowheads respectively), whereas oligomeric TDP-43 assemblies are observed in all samples between 66 kDa and 10 MDa (black brackets).

Supplementary Figure 24: Relative retention of different proteins by filtration of SarkoSpin fractions **a.** SarkoSpin supernatants and pellets from different disease types and control patients were passed through 0.22 µm syringe filters. The resulting filtrates were captured on a nitrocellulose membrane, along with the corresponding unfiltered samples for a direct comparison and immunoblotted for pTDP-43, TDP-43, and hnRNPA1. **b.** The relative reduction of signal between filtered and non-filtered fractions was calculated for each protein on four independent SarkoSpin filtration experiments.

Supplementary Figure 25: Further structural analysis of pathological TDP-43 isolated from different disease subtypes

a. TEM images of negative control, without the use of primary antibody, of immunolabeled FTLD-TDP-A insoluble material corresponding to TEM images from **Fig. 5a-b,** showing no unspecific binding of the gold-conjugated secondary antibody. Sample in panel on the left was prepared including the methylcellulose (MC) preservation step, and the sample represented on the right without the MC step. **b.** Upper panel: TEM image of immunolabeled FTLD-TDP-A aggregates with lipid contaminants surrounding the protein assemblies. Lower panel: TEM image of immunolabeled FTLD-TDP-A sample purified over sucrose cushion during SarkoSpin extraction, which efficiently removes the lipid contaminants. **c.** Representative immunoblots of SarkoSpin pellets extracted from control, ALS, FTLD-TDP-A and FTLD-TDP-C brains after proteolytic digestion. Brain homogenates were digested by different proteases for 30 minutes at 37 °C during SarkoSpin solubilization step. SarkoSpin pellets were subjected to SDS-PAGE and immunoblotted against total TDP-43 (top panels) and pTDP-43 (bottom panels). N – not treated; P – treated with 0.5 mg/ml Proteinase K; T – treated with 0.1 mg/ml Trypsin; C – treated with 0.01 mg/ml Chymotrypsin. **d.** Full size representation of the immunoblots on Chymotrypsinized and Trypsinized SarkoSpin pellets shown in **Fig. 5c**.

Supplementary Figure 26: Inoculation of phospho-GFP-TDP-43-HA SarkoSpin pellets in a doxycycline-inducible TDP-43-HA HEK293 cell line

a. Schematic representation of the pcDNA5 constructs used to generate the TDP-43-HA-expressing stable HEK293 cell line (top) and to produce SarkoSpin pellets containing phosphorylated GFP-TDP-43-HA (bottom) employed to test the inoculation conditions in the stable cell line. **b-c.** Sensitivity of the inducible system was tested by induction of TDP-43-HA expression with 1µg/ml of doxycycline for 48 hours and analyzed by Western blot (**b**) and immunofluorescence (**c**) with an HA-tag specific antibody. **d.** SarkoSpin-isolated TDP-43 aggregates in NSC-34 cells transiently transfected with the GFP-TDP-43-HA construct for 48 hours (loading: homogenate 20µg of protein, 3.3% of SarkoSpin supernatant, 20% of SarkoSpin pellet). Note that the pellet is enriched in TDP-43 and devoid from other soluble or RNA-binding proteins, with similar purity to that achieved in human brain samples. **e.** TDP-43-HA-expressing HEK293 cells internalized lipofected SarkoSpin-insoluble GFP-TDP-43-HA. 4 hours after inoculation, cells were trypsinized and collected by centrifugation before lysis in order to remove all GFP-TDP-43-HA aggregates adhered to the cell surface and only visualize those that have truly entered the cells. L2000: Lipofectamine 2000. **f.** Immunocytochemistry of TDP-43-HA-expressing cells lipofected with GFP-TDP-43-HA aggregates. Side views of the z-stack (yz plane) are depicted in 1 and 2, show examples of internalized GFP-TDP-43-HA aggregates. **g.** Immunoblots on homogenates for SarkoSpin from TDP-43-HA HEK cells inoculated with SarkoSpin pellets from control, FTLD-TDP-A or FTLD-TDP-C patients. **h.** Full-size immunoblots of SarkoSpin supernatant and pellet fractions from TDP-43-HA expressing cells inoculated with SarkoSpin pellets from control, FTLD-TDP-A or FTLD-TDP-C patients, corresponding to Figure 6c.

Supplementary Figure 27: Verification of TDP-43, pTDP-43 and total protein amounts inoculated to primary cortical neurons at 4 DIV

Normalization of total protein amounts in Sarkospin pellets inocula was achieved by BCA prior to dilution for reaching doses of 1, 0.3, 0.1 and 0.03 µg of protein per well. In parallel of the cell

treatments, an aliquot of each inoculum type and dose was loaded on dot blot and immunolabeled with antibodies against TDP-43 (**a.**), pTDP-43 pS409/410 (**b.**) and actin (**c.**). **a.** and **b.** show that TDP-43 and pTDP-43 are only present in Sarkospin pellets from FTLD patients, and at approximately double dose in FTLD-TDP-A compared to FTLD-TDP-C subtypes inocula.

Acknowledgements

We are grateful to all the patients and their families for donating tissues for scientific research; this work would not have been possible without their generosity and foresightedness. We thank Shahram Saberi and Maria J Rodriguez from UCSD for preparing and shipping autopsy material from San Diego to Zurich; Andres Käch and the Center for Microscopy and Image Analysis of the University of Zurich for help and technical support in all EM experiments; Henning Leske, Karl Frontzek, Elisabeth Rushing, Adriano Aguzzi (Institute of Neuropathology, University Hospital of Zurich) for helpful advice and discussions; Julia Luedke and Julien Weber for technical help, Sonu Sahadevan M.K. and Aurelie Zbinden for critical input on the manuscript. This work was supported by a Swiss National Science Foundation Professorship (PP00P3_144862) and a Human Frontier Science Program Career Development Award (CDA-00058/2012) to M.P. and a UCL/ZNZ Neuroscience Collaboration Grant to M.P and A.M.I funded through UCL's Wellcome Trust Institutional Strategic Support Fund 'Investing in Excellent Researchers' (105604/Z/14/Z). F.L. and M.H.P. are both recipients of the Milton-Safenowitz fellowship from the ALS Association. F.L. received a Postdoc Award and Z. M. a Candoc Award (Forschungskredit) from the University of Zurich. T.L. is funded by an Alzheimer's Research UK senior fellowship. Y.T.A. was supported by the Leonard Wolfson Centre for experimental neurology. The Queen Square Brain Bank is supported by the Reta Lila Weston Institute for Neurological Studies and the Progressive Supranuclear Palsy (Europe) Association.

Author contributions

F.L. developed and performed the biochemical experiments with the help of Z.M. and M.P. conceived and directed the study. M.P-B. generated and characterized the stable cell line with inducible TDP-43-HA, in which she performed cell toxicity experiments. M.H-P., L.G., E-M.H., and T.A. helped with performing gradients and developing the SarkoSpin method. P.B. and P.P. performed mass spectrometry, which was bioinformatically analysed by U.W.. G.B. performed electron microscopy experiments. A.A-A., A.L. and H.S. gave critical input on the structural analysis of extracted aggregates by electron microscopy and performed preliminary cryo-EM and CLEM experiments. Autopsy material and associated clinical and neuropathological information was provided by J.R., T.L. and A.I., while S.C.F. did the pTDP-43 immunohistochemistry and immunofluorescence and Y.T.A. sampled the cases from the Queen Square Brain Bank. F.DG., F.I. and E.B. performed and analyzed inoculations on primary neurons. F.L., Z.M. and M.P wrote the manuscript. All authors read, edited and approved the final manuscript.

Footnotes

Mass spectrometry raw files were uploaded to the ProteomeXchange Consortium via the PRIDE partner repository. Dataset identifier: PXD007873.

Competing financial interests

The authors declare no competing financial interests.

Literature

1. Ling, S.C., Polymenidou, M. & Cleveland, D.W. Converging mechanisms in ALS and FTD: disrupted RNA and protein homeostasis. *Neuron* **79**, 416-438 (2013).
2. Polymenidou, M. & Cleveland, D.W. Biological Spectrum of Amyotrophic Lateral Sclerosis Prions. *Cold Spring Harb Perspect Med* (2017).
3. Renton, A.E., Chio, A. & Traynor, B.J. State of play in amyotrophic lateral sclerosis genetics. *Nat Neurosci* **17**, 17-23 (2014).
4. Renton, A.E.*, et al.* A hexanucleotide repeat expansion in C9ORF72 is the cause of chromosome 9p21-linked ALS-FTD. *Neuron* **72**, 257-268 (2011).
5. DeJesus-Hernandez, M.*, et al.* Expanded GGGGCC hexanucleotide repeat in noncoding region of C9ORF72 causes chromosome 9p-linked FTD and ALS. *Neuron* **72**, 245-256 (2011).
6. Neumann, M.*, et al.* Ubiquitinated TDP-43 in frontotemporal lobar degeneration and amyotrophic lateral sclerosis. *Science* **314**, 130-133 (2006).
7. Arai, T.*, et al.* TDP-43 is a component of ubiquitin-positive tau-negative inclusions in frontotemporal lobar degeneration and amyotrophic lateral sclerosis. *Biochem Biophys Res Commun* **351**, 602-611 (2006).
8. Buratti, E.*, et al.* Nuclear factor TDP-43 and SR proteins promote in vitro and in vivo CFTR exon 9 skipping. *EMBO J* **20**, 1774-1784 (2001).
9. Polymenidou, M.*, et al.* Long pre-mRNA depletion and RNA missplicing contribute to neuronal vulnerability from loss of TDP-43. *Nat Neurosci* **14**, 459-468 (2011).
10. Tollervey, J.R.*, et al.* Characterizing the RNA targets and position-dependent splicing regulation by TDP-43. *Nat Neurosci* **14**, 452-458 (2011).
11. Afroz, T.*, et al.* Functional and dynamic polymerization of the ALS-linked protein TDP-43 antagonizes its pathologic aggregation. *Nat Commun* **8**, 45 (2017).
12. Jiang, L.L.*, et al.* The N-terminal dimerization is required for TDP-43 splicing activity. *Sci Rep* **7**, 6196 (2017).
13. Gu, J.*, et al.* Transactive response DNA-binding protein 43 (TDP-43) regulates alternative splicing of tau exon 10: Implications for the pathogenesis of tauopathies. *J Biol Chem* **292**, 10600-10612 (2017).
14. Ederle, H. & Dormann, D. TDP-43 and FUS en route from the nucleus to the cytoplasm. *FEBS Lett* **591**, 1489-1507 (2017).
15. Dewey, C.M.*, et al.* TDP-43 is directed to stress granules by sorbitol, a novel physiological osmotic and oxidative stressor. *Mol Cell Biol* **31**, 1098-1108 (2011).
16. Alami, N.H.*, et al.* Axonal transport of TDP-43 mRNA granules is impaired by ALS-causing mutations. *Neuron* **81**, 536-543 (2014).
17. Gopal, P.P., Nirschl, J.J., Klinman, E. & Holzbaur, E.L. Amyotrophic lateral sclerosis-linked mutations increase the viscosity of liquid-like TDP-43 RNP granules in neurons. *Proc Natl Acad Sci U S A* **114**, E2466-E2475 (2017).
18. Kato, M.*, et al.* Cell-free formation of RNA granules: low complexity sequence domains form dynamic fibers within hydrogels. *Cell* **149**, 753-767 (2012).

19. Molliex, A.*, et al.* Phase separation by low complexity domains promotes stress granule assembly and drives pathological fibrillization. *Cell* **163**, 123-133 (2015).

20. Igaz, L.M.*, et al.* Enrichment of C-terminal fragments in TAR DNA-binding protein-43 cytoplasmic inclusions in brain but not in spinal cord of frontotemporal lobar degeneration and amyotrophic lateral sclerosis. *Am J Pathol* **173**, 182-194 (2008).

21. Neumann, M.*, et al.* Phosphorylation of S409/410 of TDP-43 is a consistent feature in all sporadic and familial forms of TDP-43 proteinopathies. *Acta Neuropathol* **117**, 137-149 (2009).

22. Lagier-Tourenne, C., Polymenidou, M. & Cleveland, D.W. TDP-43 and FUS/TLS: emerging roles in RNA processing and neurodegeneration. *Hum Mol Genet* **19**, R46-64 (2010).

23. Guo, W.*, et al.* An ALS-associated mutation affecting TDP-43 enhances protein aggregation, fibril formation and neurotoxicity. *Nat Struct Mol Biol* **18**, 822-830 (2011).

24. Johnson, B.S.*, et al.* TDP-43 is intrinsically aggregation-prone, and amyotrophic lateral sclerosis-linked mutations accelerate aggregation and increase toxicity. *J Biol Chem* **284**, 20329-20339 (2009).

25. Arnold, E.S.*, et al.* ALS-linked TDP-43 mutations produce aberrant RNA splicing and adult-onset motor neuron disease without aggregation or loss of nuclear TDP-43. *Proc Natl Acad Sci U S A* **110**, E736-745 (2013).

26. Laferriere, F. & Polymenidou, M. Advances and challenges in understanding the multifaceted pathogenesis of amyotrophic lateral sclerosis. *Swiss Med Wkly* **145**, w14054 (2015).

27. Neary, D.*, et al.* Frontotemporal lobar degeneration: a consensus on clinical diagnostic criteria. *Neurology* **51**, 1546-1554 (1998).

28. Mackenzie, I.R. & Neumann, M. Reappraisal of TDP-43 pathology in FTLD-U subtypes. *Acta Neuropathol* **134**, 79-96 (2017).

29. Lee, E.B.*, et al.* Expansion of the classification of FTLD-TDP: distinct pathology associated with rapidly progressive frontotemporal degeneration. *Acta Neuropathol* **134**, 65-78 (2017).

30. Lashley, T., Rohrer, J.D., Mead, S. & Revesz, T. Review: an update on clinical, genetic and pathological aspects of frontotemporal lobar degenerations. *Neuropathol Appl Neurobiol* **41**, 858-881 (2015).

31. Nonaka, T.*, et al.* Prion-like properties of pathological TDP-43 aggregates from diseased brains. *Cell Rep* **4**, 124-134 (2013).

32. Tsuji, H.*, et al.* Molecular analysis and biochemical classification of TDP-43 proteinopathy. *Brain* **135**, 3380-3391 (2012).

33. Laferriere, F.*, et al.* Quaternary structure of pathological prion protein as a determining factor of strain-specific prion replication dynamics. *PLoS Pathog* **9**, e1003702 (2013).

34. Polymenidou, M.*, et al.* Coexistence of multiple PrPSc types in individuals with Creutzfeldt-Jakob disease. *Lancet Neurol* **4**, 805-814 (2005).

35. Carra, S.*, et al.* Alteration of protein folding and degradation in motor neuron diseases: Implications and protective functions of small heat shock proteins. *Prog Neurobiol* **97**, 83-100 (2012).

36. Neumann, M., *et al.* Absence of heterogeneous nuclear ribonucleoproteins and survival motor neuron protein in TDP-43 positive inclusions in frontotemporal lobar degeneration. *Acta Neuropathol* **113**, 543-548 (2007).

37. Kametani, F., *et al.* Mass spectrometric analysis of accumulated TDP-43 in amyotrophic lateral sclerosis brains. *Sci Rep* **6**, 23281 (2016).

38. Ingre, C., *et al.* A novel phosphorylation site mutation in profilin 1 revealed in a large screen of US, Nordic, and German amyotrophic lateral sclerosis/frontotemporal dementia cohorts. *Neurobiol Aging* **34**, 1708 e1701-1706 (2013).

39. Wu, C.H., *et al.* Mutations in the profilin 1 gene cause familial amyotrophic lateral sclerosis. *Nature* **488**, 499-503 (2012).

40. Zhou, J., *et al.* Spinal muscular atrophy associated with progressive myoclonic epilepsy is caused by mutations in ASAH1. *Am J Hum Genet* **91**, 5-14 (2012).

41. Xu, G., Stevens, S.M., Jr., Moore, B.D., McClung, S. & Borchelt, D.R. Cytosolic proteins lose solubility as amyloid deposits in a transgenic mouse model of Alzheimer-type amyloidosis. *Hum Mol Genet* **22**, 2765-2774 (2013).

42. McGurk, L., *et al.* Poly-A binding protein-1 localization to a subset of TDP-43 inclusions in amyotrophic lateral sclerosis occurs more frequently in patients harboring an expansion in C9orf72. *J Neuropathol Exp Neurol* **73**, 837-845 (2014).

43. Kerman, A., *et al.* Amyotrophic lateral sclerosis is a non-amyloid disease in which extensive misfolding of SOD1 is unique to the familial form. *Acta Neuropathol* **119**, 335-344 (2010).

44. Robinson, J.L., *et al.* TDP-43 skeins show properties of amyloid in a subset of ALS cases. *Acta Neuropathol* **125**, 121-131 (2013).

45. Lin, W.L. & Dickson, D.W. Ultrastructural localization of TDP-43 in filamentous neuronal inclusions in various neurodegenerative diseases. *Acta Neuropathol* **116**, 205-213 (2008).

46. Guenther, E.L., *et al.* Atomic structures of TDP-43 LCD segments and insights into reversible or pathogenic aggregation. *Nat Struct Mol Biol* **25**, 463-471 (2018).

47. Aguzzi, A., Heikenwalder, M. & Polymenidou, M. Insights into prion strains and neurotoxicity. *Nature reviews. Molecular cell biology* **8**, 552-561 (2007).

48. Yagi, H., *et al.* Zonisamide Enhances Neurite Elongation of Primary Motor Neurons and Facilitates Peripheral Nerve Regeneration In Vitro and in a Mouse Model. *PLoS One* **10**, e0142786 (2015).

49. Danzer, K.M., Krebs, S.K., Wolff, M., Birk, G. & Hengerer, B. Seeding induced by alpha-synuclein oligomers provides evidence for spreading of alpha-synuclein pathology. *J Neurochem* **111**, 192-203 (2009).

50. Polymenidou, M. & Cleveland, D.W. The seeds of neurodegeneration: prion-like spreading in ALS. *Cell* **147**, 498-508 (2011).

51. Sanders, D.W., *et al.* Distinct tau prion strains propagate in cells and mice and define different tauopathies. *Neuron* **82**, 1271-1288 (2014).

52. Peelaerts, W., *et al.* alpha-Synuclein strains cause distinct synucleinopathies after local and systemic administration. *Nature* **522**, 340-344 (2015).

53. Meyer-Luehmann, M.*, et al.* Exogenous induction of cerebral beta-amyloidogenesis is governed by agent and host. *Science* **313**, 1781-1784 (2006).

54. Leek, J.T., Johnson, W.E., Parker, H.S., Jaffe, A.E. & Storey, J.D. The sva package for removing batch effects and other unwanted variation in high-throughput experiments. *Bioinformatics* **28**, 882-883 (2012).

55. Ling, S.C.*, et al.* ALS-associated mutations in TDP-43 increase its stability and promote TDP-43 complexes with FUS/TLS. *Proc Natl Acad Sci U S A* **107**, 13318-13323 (2010).

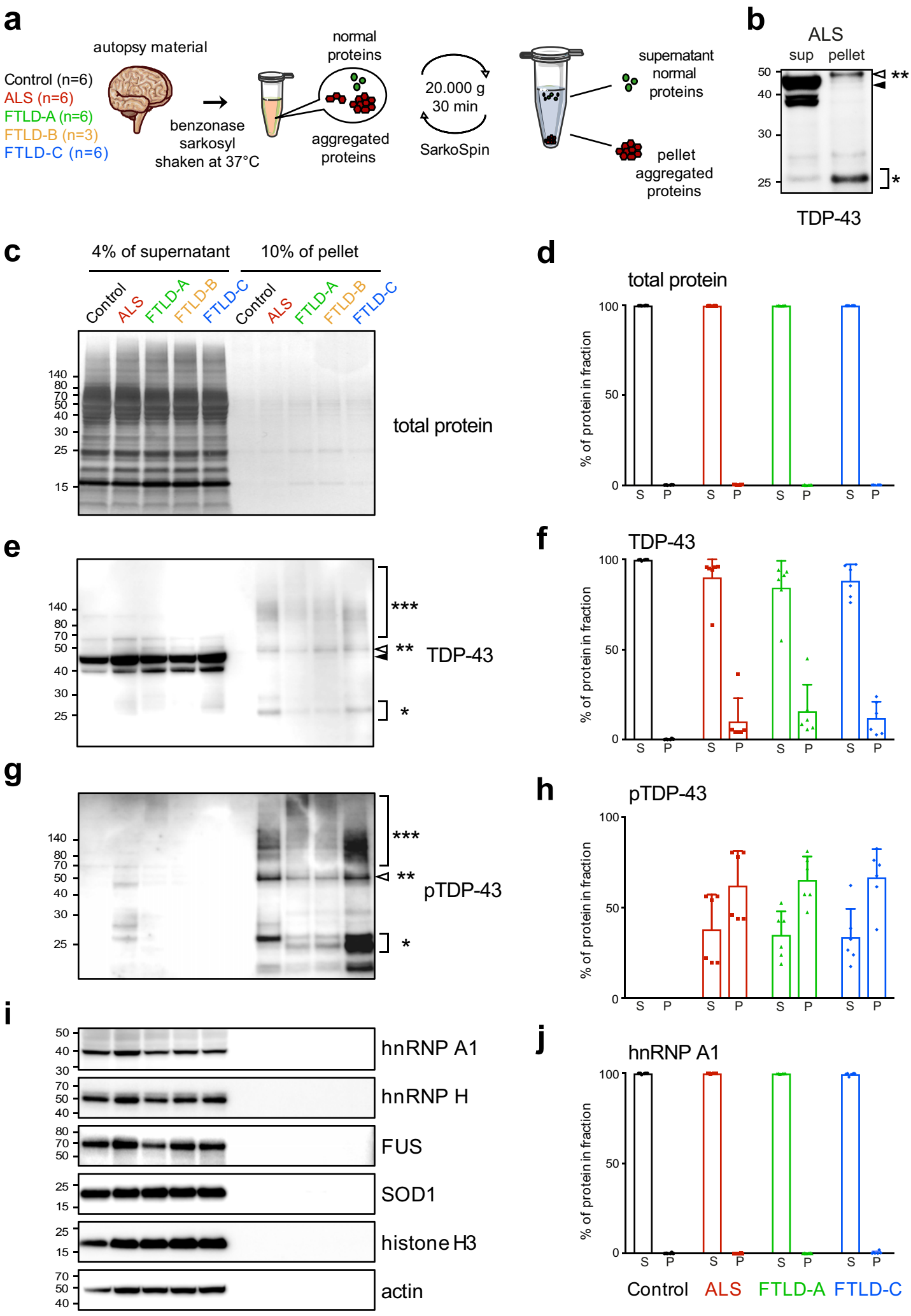

Laferriere et al. Figure 1

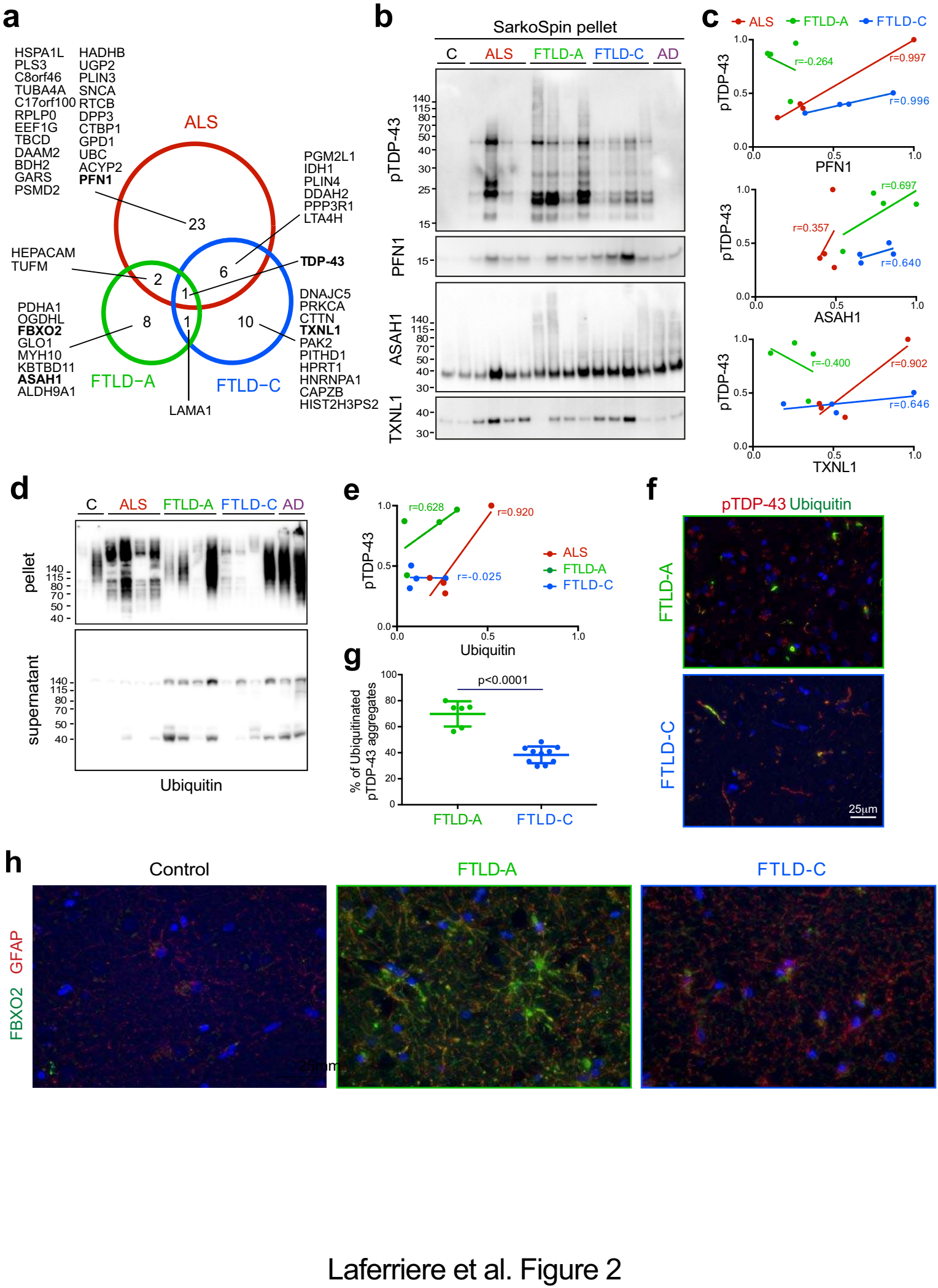

Laferriere et al. Figure 2

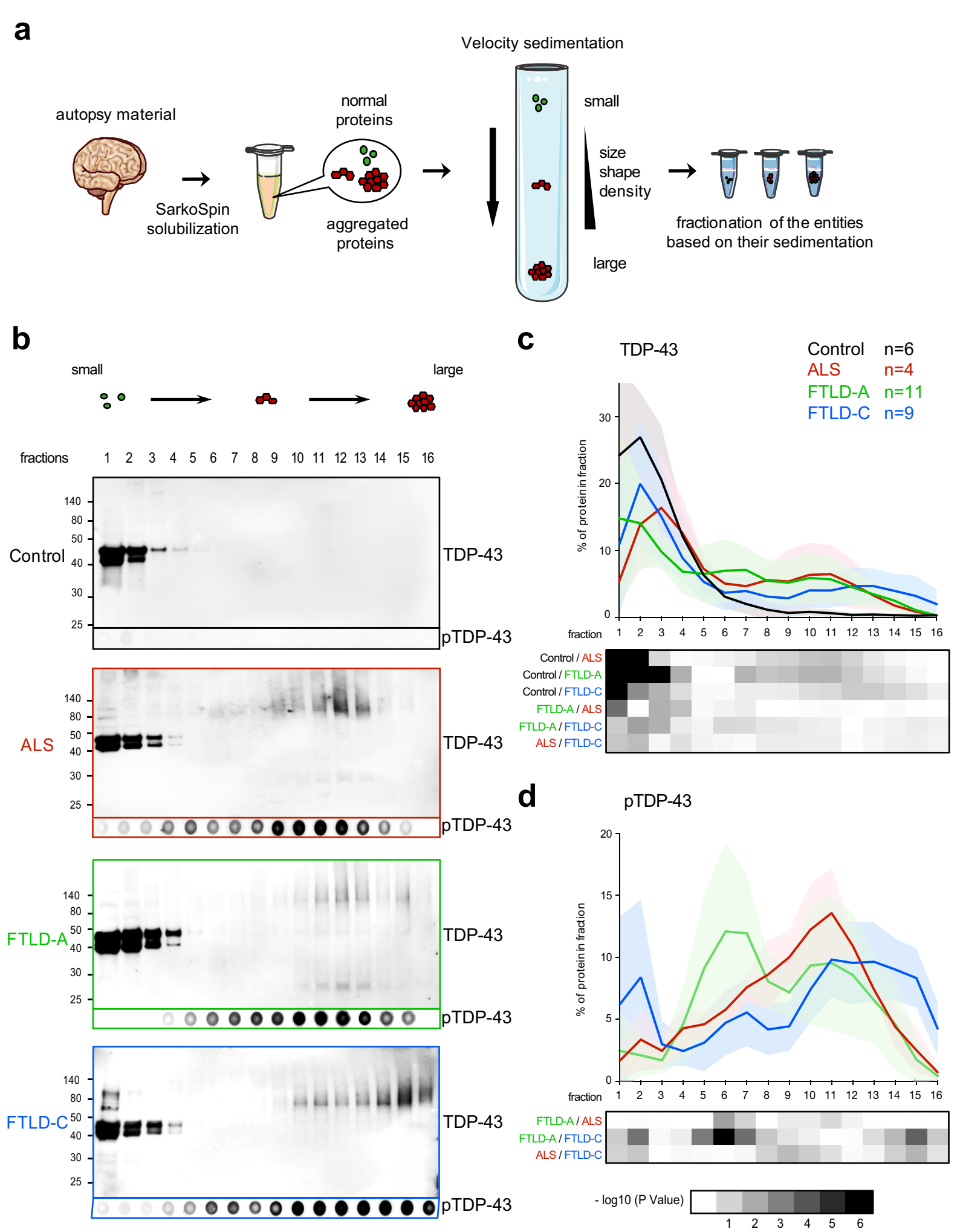

Laferriere et al. Figure 3

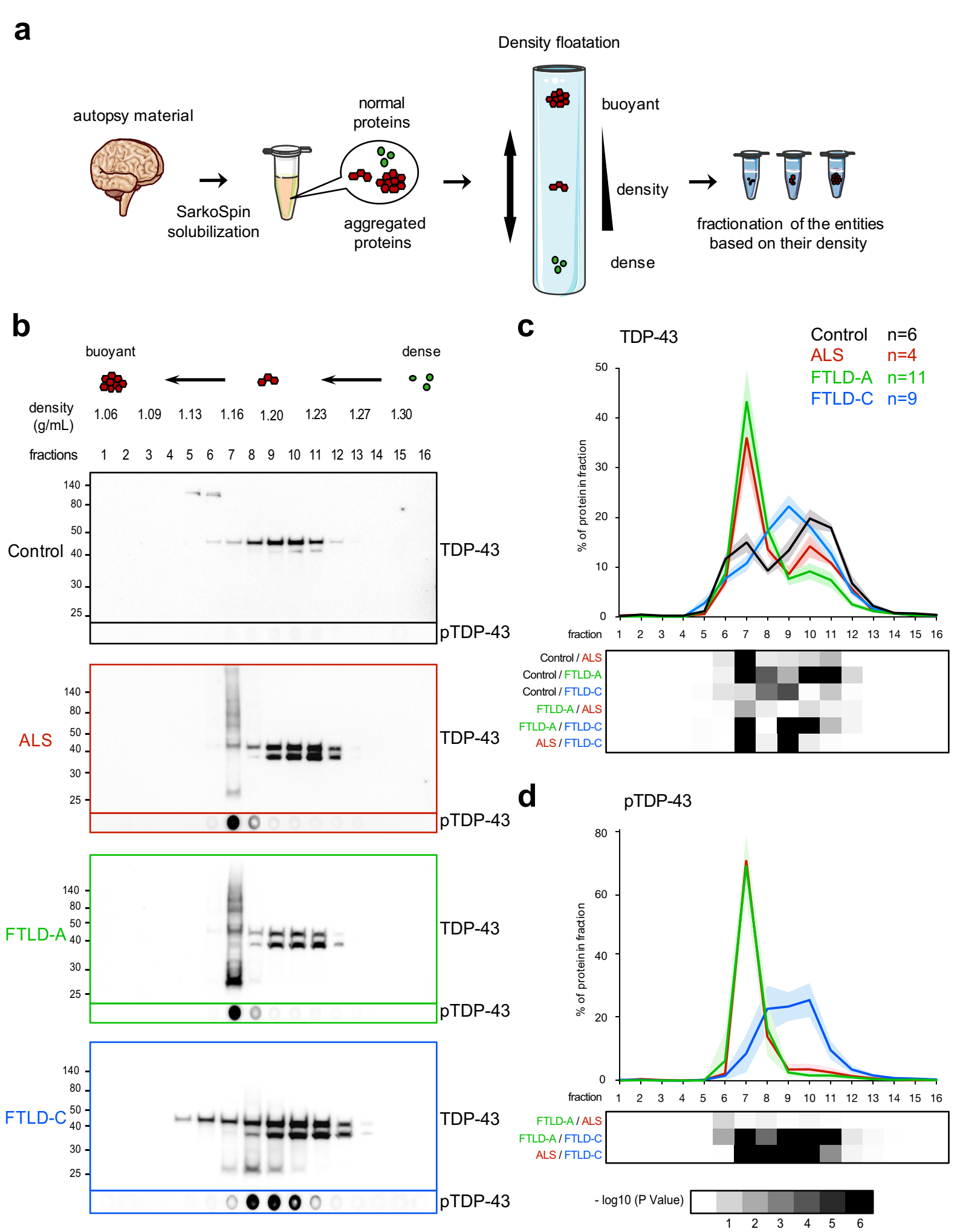

Laferriere et al. Figure 4

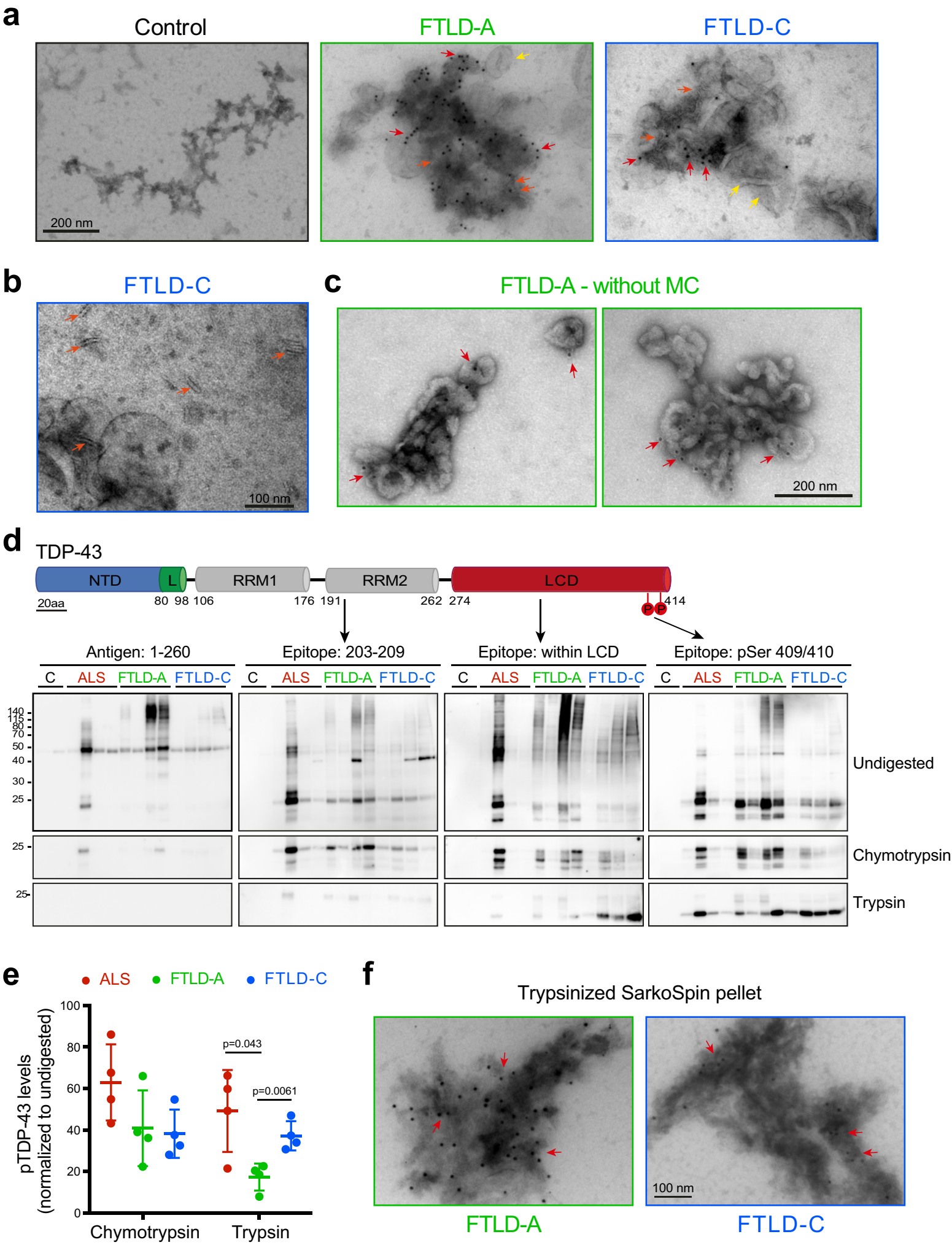

Laferriere et al. Figure 5

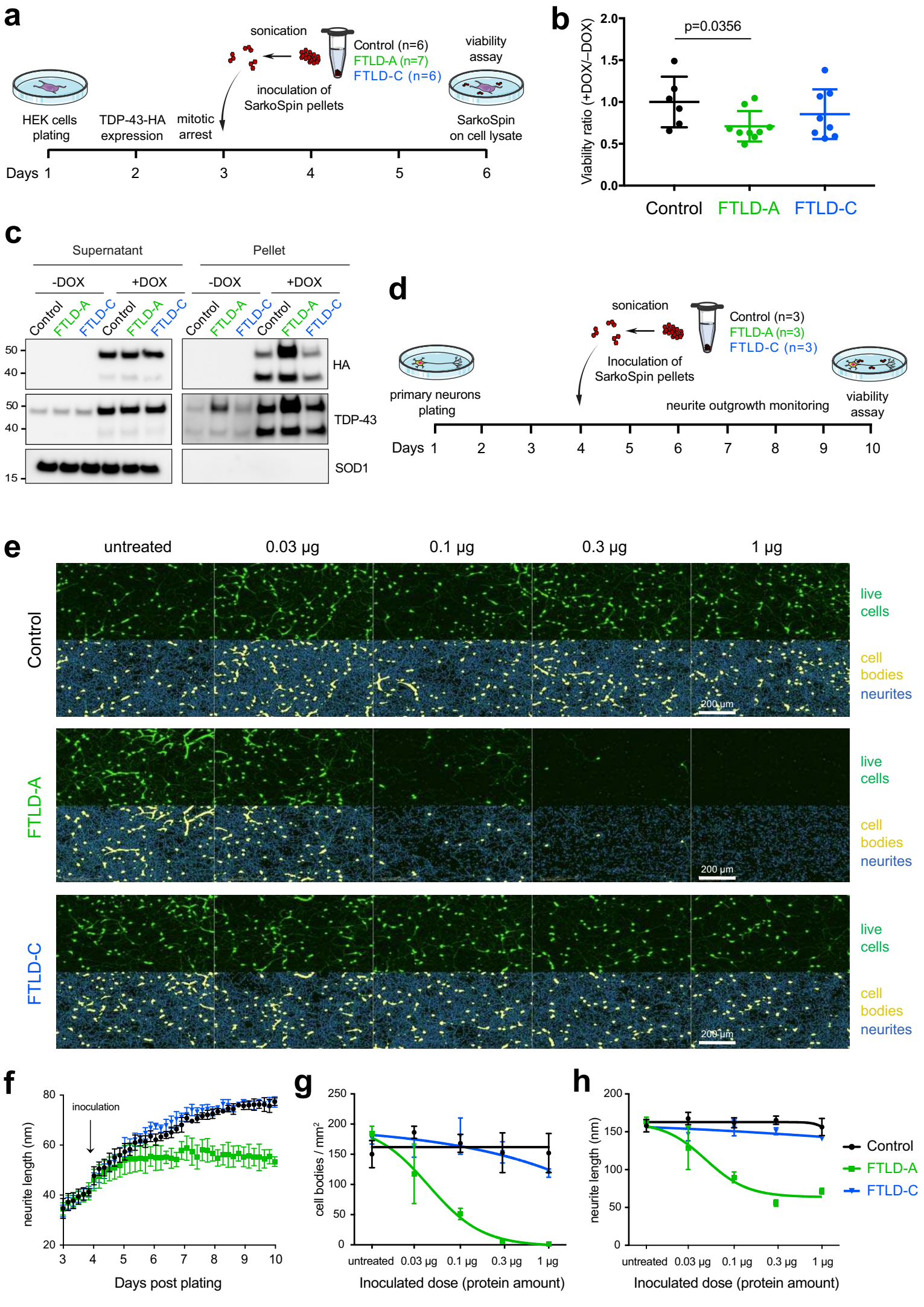

Laferriere et al. Figure 6